THE JOURNAL OF BIOLOGICAL CHEMISTRY VOL. 290, NO. 37, pp. 22699–22714, September 11, 2015

Phosphorylation-dependent Changes in Nucleotide Binding, Conformation, and Dynamics of the First Nucleotide Binding Domain (NBD1) of the Sulfonylurea Receptor 2B (SUR2B)*

Received for publication, January 23, 2015, and in revised form, July 20, 2015 Published, JBC Papers in Press, July 21, 2015, DOI 10.1074/jbc.M114.636233

Elvin D. de Araujo[‡§1], Claudia P. Alvarez[‡§], Jorge P. López-Alonso[‡§¶2], Clarissa R. Sooklal[‡§], Marijana Stagljar[‡§¶], and Voula Kanelis[‡§¶3]

From the [‡]Department of Chemical and Physical Sciences, University of Toronto Mississauga, Mississauga, Ontario L5L 1C6, the [§]Department of Chemistry, University of Toronto, Toronto, Ontario M5S 3H6, and the [¶]Department of Cell and Systems Biology, University of Toronto, Toronto, Ontario M5S 3G5, Canada

Background: Phosphorylation of SUR2B NBD1 activates ATP-sensitive K^+ (K_{ATP}) channels.
Results: Phosphorylation-dependent changes in NBD1 conformation and nucleotide binding are mimicked by removing the N-terminal tail that contains the phosphorylation sites.
Conclusion: Phosphorylation disrupts interactions of the N-terminal tail with the NBD1 core, leading to increased nucleotide binding.
Significance: These data provide insights into the molecular basis by which NBD1 phosphorylation activates K_{ATP} channels.

The sulfonylurea receptor 2B (SUR2B) forms the regulatory subunit of ATP-sensitive potassium (K_{ATP}) channels in vascular smooth muscle. Phosphorylation of the SUR2B nucleotide binding domains (NBD1 and NBD2) by protein kinase A results in increased channel open probability. Here, we investigate the effects of phosphorylation on the structure and nucleotide binding properties of NBD1. Phosphorylation sites in SUR2B NBD1 are located in an N-terminal tail that is disordered. Nuclear magnetic resonance (NMR) data indicate that phosphorylation of the N-terminal tail affects multiple residues in NBD1, including residues in the NBD2-binding site, and results in altered conformation and dynamics of NBD1. NMR spectra of NBD1 lacking the N-terminal tail, NBD1-ΔN, suggest that phosphorylation disrupts interactions of the N-terminal tail with the core of NBD1, a model supported by dynamic light scattering. Increased nucleotide binding of phosphorylated NBD1 and NBD1-ΔN, compared with non-phosphorylated NBD1, suggests that by disrupting the interaction of the NBD core with the N-terminal tail, phosphorylation also exposes the MgATP-binding site on NBD1. These data provide insights into the molecular basis by which phosphorylation of SUR2B NBD1 activates K_{ATP} channels.

ATP-sensitive potassium (K_{ATP})[4] channels are K^+-selective channels present in many tissues (1). Because gating of K_{ATP} channels depends on the cellular concentrations of ATP and ADP, K_{ATP} channels couple cellular metabolism to membrane potential (2). Thus, K_{ATP} channels play critical roles in several biological processes, such as insulin secretion in the pancreas (3), neurotransmitter release in the brain (3), cardiac function, and regulation of blood pressure (1).

K_{ATP} channels are multimeric protein complexes composed of four copies of a pore-forming inward-rectifying potassium channel (Kir6.2 or Kir6.1) and four copies of a sulfonylurea receptor (SUR1, SUR2A, or SUR2B) that surround the pore (1, 4). Different combinations of SUR and Kir6.x proteins combine to form K_{ATP} channels in different tissues. The SUR proteins are members of the ATP-binding cassette (ABC) superfamily of proteins (5), which consist of a minimum of two membrane spanning domains (MSD1 and MSD2) and two nucleotide binding domains (NBD1 and NBD2) (Fig. 1*A*). Binding of MgATP leads to dimerization of the NBD1 and NBD2, which dissociate upon MgATP hydrolysis (6). In addition to the minimum ABC protein structure, the SUR proteins contain a third membrane spanning domain (MSD0) that is linked to the N terminus of MSD1 by the cytoplasmic L0 linker (7–10). Unlike most members of the family, SUR proteins possess no known transporter activity but instead regulate gating of the Kir6.x

* This work was supported in part by Canadian Institutes of Health Research Grant MOP-106470 and the Natural Sciences and Engineering Council of Canada Grant RGPIN 357118-09 (to V. K.). The authors declare that they have no conflicts of interest with the contents of this article.

NMR resonance assignments for NBD1-ΔN have been deposited in the BioMag Res Bank under BMRB accession code 26615.

[1] Supported by a Frederick Banting and Charles Best Canada Graduate Scholarship from the Canadian Institutes of Health Research.

[2] Supported by an Ontario Postdoctoral Fellowship. Present address: CIC bioGUNE, Edificio 800, Parque Tecnológico de Bizkaia, 48160 Derio (Bizkaia), Spain.

[3] Supported by an Early Researcher Award from the Ontario Ministry of Economic Development and Innovation and a Canadian Institutes of Health Research New Investigator Award. To whom correspondence should be addressed: DV 4042 Department of Chemical and Physical Sciences, University of Toronto Mississauga, 3359 Mississauga Road N., Mississauga, Ontario L5L 1C6. Tel.: 905-569-4542; Fax: 905-828-5425; E-mail: voula.kanelis@utoronto.ca.

[4] The abbreviations used are: K_{ATP} channel, ATP-sensitive potassium channel; ABC, ATP-binding cassette; SUR, sulfonylurea receptor; CFTR, cystic fibrosis transmembrane conductance regulator; HSQC, heteronuclear single quantum coherence; NBD, nucleotide binding domain; SUMO, small ubiquitin-like modifier; TNP-ATP, 2′,3′-*O*-(2,4,6-trinitrophenyl)adenosine-5′-triphosphate; TROSY, transverse relaxation optimized spectroscopy; Ulp1, (ubiquitin-like protein)-specific protease 1.

pore. ATP binding at the Kir6.x pore results in K_{ATP} channel inhibition, whereas nucleotide binding and/or hydrolysis at the SUR NBDs results in channel opening (11). Data on full-length channels indicate that K_{ATP} channels open in response to MgATP binding at NBD1 and MgADP binding at NBD2 (12). The interaction of NBD2 with MgADP may result from direct nucleotide binding or hydrolysis of MgATP to MgADP at NBD2 (2, 12). The SUR NBDs are critical in regulating K_{ATP} channel gating. Mutations in the NBDs of SUR1 cause neonatal type II diabetes or hyperinsulinism (13), whereas mutations in the NBDs of SUR2A and SUR2B result in various cardiovascular disorders (14–18).

Although nucleotide binding and/or hydrolysis at the NBDs are sufficient to induce channel currents, K_{ATP} channel activity is also affected by phosphorylation of SUR and/or Kir6.x subunits (19–27). In the case of vascular K_{ATP} channels, monophosphorylation of murine SUR2B at three sites (Thr-633 and Ser-1465 (24) or Ser-1387 (26)) by protein kinase A (PKA) results in K_{ATP} channel activation, with di-phosphorylation of Thr-633 and Ser-1465 further stimulating channel activity (24). Notably, the phosphorylation sites are conserved among species (Thr-635, Ser-1390, and Thr-1547, respectively, in human SUR2B), highlighting their importance in regulating the activity of the SUR NBDs and their subsequent control of K_{ATP} channel function. A molecular level understanding of how phosphorylation activates K_{ATP} channels is not available but may involve altered MgATP binding and hydrolysis and/or intra- and intermolecular interactions of the NBDs, as seen for the cystic fibrosis transmembrane conductance regulator (CFTR) (28–31).

Here, we present experiments detailing the effect of phosphorylation on the conformation and nucleotide binding of rat SUR2B NBD1. The sequence of rat SUR2B NBD1 is ~96% identical to human SUR2B NBD1, including the phosphorylation site Thr-632 (Thr-635 in human SUR2B), with most amino acid changes occurring in unstructured loops (32). The studies presented here employed four different SUR2B NBD1-containing constructs (Fig. 1*B*). 1) The complete SUR2B NBD1 (NBD1) consists of residues Ser-615–Leu-933 and is a folded and functional protein domain that possesses a predicted disordered N-terminal tail, which contains the Thr-632 phosphorylation site and a predicted disordered C-terminal tail (32). 2) SUR2B NBD1 from Ser-615–Asp-914 (NBD1-ΔC) lacks the C-terminal tail. 3) SUR2B NBD1 from Asp-665–Leu-933 (NBD1-ΔN) lacks the N-terminal tail. 4) SUR2B NBD1 from Asp-665–Asp-914 (NBD1-ΔNΔC) lacks the N- and C-terminal tails and includes only the canonical NBD1 fold. We also used a SUR2B construct composed of the isolated N-terminal tail (Ser-615–Glu-664), herein referred to as the N-tail. We have obtained resonance assignments for NBD1 and have probed conformational changes in NBD1 with phosphorylation. Data from NMR spectroscopy and dynamic light scattering suggest that the N-terminal tail interacts with multiple residues in NBD1, including residues in the NBD2-binding site, and that phosphorylation of the N-terminal tail disrupts its interactions with the core of NBD1. Because the N-terminal tail is ~50 residues long (Fig. 1), it has the potential to adopt multiple conformations, including conformations that are bound to NBD1. Fluorescence studies demonstrate increased nucleotide binding affinity of phosphorylated NBD1 (phospho-NBD1) and NBD1-ΔN. These findings provide insights into the molecular basis by which phosphorylation of NBD1 activates K_{ATP} channel gating.

Experimental Procedures

Protein Expression and Purification—Wild type rat SUR2B NBD1 proteins comprising residues Ser-615–Leu-933 (NBD1), Ser-615–Asp-914 (NBD1-ΔC), Asp-665–Leu-933 (NBD1-ΔN), Asp-665–Asp-914 (NBD1-ΔNΔC), and Ser-615–Glu-664 (N-tail) were prepared as described previously (32, 33). We also prepared samples of NBD1 and NBD1-ΔN with mutations of Trp residues. Briefly, the SUR2B NBD1, NBD1-ΔC, NBD1-ΔN, NBD1-ΔNΔC, and N-tail proteins were expressed as fusions with a cleavable N-terminal His_6-SUMO tag in *Escherichia coli* BL21 (DE3) CodonPlus-RIL (Stratagene) cells. Uniformly ^{15}N-labeled SUR2B NBD1 proteins were expressed in cells grown in 97.5% ^{15}N-labeled M9 minimal media and 2.5% ^{15}N-labeled *E. coli*-OD2 media (Silantes). SUR2B NBD1-ΔN samples used for NMR resonance assignment experiments were grown in 97.5% M9 minimal media (containing $^{15}NH_4Cl$, [^{13}C]glucose, and 70% ^2H_2O) and 2.5% $^{15}N/^{13}C$-labeled *E. coli*-OD2 media (Silantes) to achieve uniform $^{15}N/^{13}C$ labeling and fractional ^2H labeling. Uniformly ^{15}N-labeled SUR2B N-tail samples were expressed in cells grown in 100% ^{15}N-labeled M9 minimal media. All protein purification steps were conducted at 4 °C. The His_6-SUMO fusion proteins were isolated using a Ni^{2+}-nitrilotriacetic acid (NTA) affinity column (GE Healthcare), and the His_6-SUMO tag was cleaved with His_6-Ulp1 protease. The SUR2B NBD1, NBD1-ΔC, NBD1-ΔN, NBD1-ΔNΔC, and N-tail proteins were next purified to homogeneity by size exclusion chromatography (Superdex 75, GE Healthcare), followed by a reverse Ni^{2+}-NTA affinity column to remove small amounts of the His_6-SUMO and/or His_6-Ulp1 proteins that co-elute with the NBD and N-tail proteins from the size exclusion column. For the NMR phosphorylation and fluorescence studies, the SUR2B NBD1, NBD1-ΔC, NBD1-ΔN, and NBD1-ΔNΔC proteins were exchanged into NBD1 buffer (20 mM sodium phosphate, pH 7.3, 150 mM NaCl, 2% (v/v) glycerol, 2 mM DTT) with and without ATP and $MgCl_2$, as required. Samples were exchanged by dialysis against the same stock of NBD1 buffer to ensure the solution conditions of the samples were identical. For the resonance assignment experiments, the NBD1-ΔN sample was exchanged into the NBD1 buffer containing 5 mM MgATP and 5 mM DTT and lacking NaCl, as the protein is more stable without salt (33). The N-tail was exchanged into a buffer identical to the NBD1 buffer but which lacked MgATP and contained 2 mM tris(2-carboxyethyl)phosphine-HCl rather than DTT.

NMR Spectroscopy—TROSY-HSQC spectra (34) of SUR2B NBD1, NBD1-ΔC, NBD1-ΔN, and NBD1-ΔNΔC were recorded at 20, 25, and/or 30 °C on a 600 MHz Varian Inova spectrometer equipped with an H(F)CN triple resonance cryoprobe and actively shielded *z*-gradients. For direct comparison with NBD1 and NBD1-ΔC, TROSY-HSQC spectra, rather than standard HSQC spectra, were also recorded of the N-tail. Chemical shifts for each spectrum were referenced to 4,4-dimethyl-4-silapentane-1-sulfonic acid (35). Spectra were pro-

cessed using NMRPipe/NMRDraw (36) and analyzed with NMRView (37). Chemical shift changes with phosphorylation or removal of the N-terminal tail were determined by calculating the combined chemical shift difference in Hz, $\Delta\delta_{tot}$, from the equation $\Delta\delta_{tot} = (\Delta\delta_{HN}{}^2 + \Delta\delta_{N}{}^2)^{0.5}$ (33, 38). When assessing chemical shift differences, only resonances exhibiting a significantly combined chemical shift difference ($\Delta\delta_{tot}$), which is greater than the average of all $\Delta\delta_{tot}$ values plus one standard deviation, are considered. For NMR data presented in this paper, only $\Delta\delta_{tot} \geq 8$ Hz is considered.

Backbone ^{1}H, ^{15}N, ^{13}C, and $^{13}C\alpha$, and side chain $^{13}C\beta$ resonance assignments for NBD1-ΔN were obtained from standard triple resonance TROSY-based experiments (39, 40) recorded on samples of 0.5 mM NBD1-ΔN that were uniformly ^{15}N- and ^{13}C-labeled and fractionally ^{2}H-labeled to ~50%. The triple resonance assignment data were run on an 800 MHz spectrometer equipped with a cryoprobe (QANUC NMR Facility, McGill University) or on a 600 MHz spectrometer equipped with an H(F)CN room temperature probe at 25 °C. These data were supplemented with ^{15}N-^{1}H TROSY HSQC spectra recorded on samples that were either ^{15}N-labeled only on specific amino acids (Gly, Leu, Ser, and Val) (31, 41, 42) or ^{14}N-labeled on specific amino acids (Ala, Arg, His, Lys, Met, and Thr) and ^{15}N-labeled at all other positions (43). Spectra of the specifically labeled NBD1-ΔN samples were recorded at 25 °C at 600 MHz. Resonance assignments of NBD1-ΔN spectra at 25 °C were transferred to NBD1-ΔN and NBD1-ΔNΔC spectra at 30 °C and then subsequently to phospho-NBD1 and phospho-NBD1-ΔC spectra at 30 °C. The similarity of the NBD1-ΔN spectrum to the spectra of other NBD1-containing proteins allowed for the straightforward transfer of resonance assignments for most residues. We have obtained assignments for 58–63% of backbone HN resonances of the NBD1-containing proteins. The combination of TROSY-based triple resonance data and specifically labeled samples has allowed for the level of resonance assignment obtained for other NBDs (31). Assignments of Trp indole HN resonances were obtained by site-directed mutagenesis of NBD1 or NBD1-ΔN.

Phosphorylation of NBD1 (Ser-615–Leu-933), NBD1-ΔC (Ser-615–Asp-914), and N-tail—Phosphorylation reactions were carried out at 30 °C on purified samples of NBD1, NBD1-ΔC, and N-tail (~200 μM) in the NBD1 buffer with 15 mM MgATP rather than 5 mM MgATP. The phosphorylation reaction was initiated by the addition of 750 units (or 0.6 μM) of the catalytic subunit of protein kinase A (PKA, Promega) and was monitored by recording a series of two-dimensional ^{1}H-^{15}N TROSY-HSQC spectra at 30 °C. The NBD1 phosphorylation reaction was allowed to proceed for 16 h, at which point the NBD1 sample was almost fully phosphorylated (>97%), as determined by the peak intensities of a resonance corresponding to the indole HN group of Trp-616 in the non-phosphorylated and phosphorylated states. Phosphorylation of N-tail was allowed to proceed for 6 h. Phosphorylation sites were identified by mass spectrometry following in-gel tryptic digestion (Advanced Protein Technology Centre, Hospital for Sick Children). The phosphorylated NBD1 and NBD1-ΔC were exchanged into the NBD1 buffer, which contained 5 mM MgATP, by size exclusion chromatography. The phosphorylated N-tail was exchanged into the N-tail buffer.

Fluorescence Nucleotide Binding Experiments—The K_d value for binding of the fluorescent ATP analogue TNP-ATP (Molecular Probes) to phosphorylated NBD1 and NBD1-ΔN was determined and compared with binding to NBD1, as done previously (33, 44). The fluorescence nucleotide binding studies were performed on a Fluoromax-4 spectrofluorimeter (Horiba-Jovin, Inc.) equipped with a Peltier unit for precise temperature control. Mg^{2+} and ATP were removed from the NBD1 samples using size exclusion chromatography and replaced with 2.5 μM $MgCl_2$ and 2.5 μM TNP-ATP. Because of the limited solubility of nucleotide-free NBD1 samples, binding experiments were conducted using 10% (v/v) glycerol at 15 °C. Binding experiments were performed by serial dilutions of the protein from 50 to 70 μM, depending on the concentration eluted from the size exclusion column, to 0.8 to 2.0 μM while keeping the concentrations of the $MgCl_2$ and TNP-ATP constant at 2.5 μM each. A separate sample was generated containing $MgCl_2$, TNP-ATP, and buffer only for the 0 mM NBD1 sample. Fluorescence emission spectra (from 485 to 600 nm) of TNP-ATP were recorded immediately after each sample was generated using an excitation wavelength of 465 nm, an excitation slit width of 5 nm, and an emission slit width of 7 nm. The K_d value for the NBD1-nucleotide complex was determined by monitoring the ratio between the fluorescence intensity at 533 nm, which corresponds to the wavelength where the fluorescence difference of free and bound TNP-ATP is at a maximum, and 600 nm to account for any nonspecific fluorescence from the protein (45). The titration data were fit to the equation

$$I = I_0 + \frac{(I_\infty - I_0)}{2[TNP_{total}]}\{([TNP_{total}] + [NBD1_{total}] + K_d) - (([TNP_{total}] + [NBD1_{total}] + K_d)^2 - (4[TNP_{total}][NBD1_{total}]))^{0.5}\} \quad \text{(Eq. 1)}$$

where I is the fluorescence intensity ratio at a given total concentration of TNP-ATP ($[TNP_{total}]$); I_∞ is the fluorescence intensity ratio at saturation; I_0 is the fluorescence intensity ratio in the absence of ligand; K_d is the dissociation constant, and $[NBD1_{total}]$ is the total concentration of SUR2B NBD1 in the reaction. Equation 1 assumes a 1:1 complex of NBD1 with TNP-ATP (46, 47).

Thermal Stability Measurements—The thermal stabilities of the NBD1 proteins were measured using intrinsic Trp fluorescence spectroscopy, as described previously (33). Briefly, thermal denaturation was monitored by following the change in the emission spectrum at 350 nm, the wavelength at which the difference in the fluorescence spectra of the folded and denatured proteins is at a maximum. The excitation wavelength was 295 nm, and the excitation and emission slit widths were 1 and 3 nm, respectively. The NBD1 proteins were heated from 10 to 60 °C in 1 °C increments, with a 1-min equilibration time at each temperature. The fluorescence emission at 350 nm was recorded at each temperature in a 0.5-ml cuvette. Thermal denaturation studies were done with 2 μM NBD1 in the absence and presence of 2 mM MgATP.

Dynamic Light Scattering Studies—Dynamic light scattering experiments were performed on a Malvern Zetasizer NanoZS

instrument with 100 μM samples of non-phospho-NBD1, phospho-NBD1, and NBD1-ΔN in the NBD1 buffer containing 2 mM MgATP. Samples were centrifuged for 10 min at 15,000 rpm prior to each experiment. The hydrodynamic radius was determined from the average of the frequency distribution of particle sizes in three separate experiments for each sample.

Results

Identification of Phosphorylation Sites in SUR2B NBD1—Phosphorylation of SUR2B NBD1, NBD1-ΔC, and N-tail *in vitro* was achieved by incubating purified proteins with the catalytic subunit of PKA, the *in vivo* kinase for the SUR proteins (24, 26). Deletion of residues Gln-915–Leu-933 from NBD1 to form NBD1-ΔC results in the disappearance of 15 intense resonances centered about 8.2 ppm in the ^{1}H dimension (Fig. 2*A*, highlighted with a +), confirming previous predictions that the C-terminal tail is disordered (32). Removal of the C-terminal tail thereby results in reduced resonance overlap in the NMR spectrum, making it possible to see additional chemical shift changes upon phosphorylation with NBD1-ΔC compared with NBD1 (see below). Although disordered, the C-terminal tail residues Gln-915–Leu-933 significantly enhance the solubility of NBD1 (32). Furthermore, residues outside the canonical NBD fold are often involved in regulation of the NBD function (28, 48, 49).

NMR spectra of the isolated N-tail indicate that, as predicted (32), residues Ser-615–Glu-664 are also disordered (Fig. 2*B*). The N-tail used here is part of the intracellular linker (Gln-600–Glu-664) connecting transmembrane helix 11 to NBD1 (Fig. 1*A*). Transmembrane helix predictions (50), sequence alignments (38, 44), and homology models (44) of SUR2B based on structures of other ABC proteins (51–57) indicate that transmembrane helix 11 ends at Val-599, that residues Gln-600–Leu-607 extend transmembrane helix 11 into the cytoplasm, and that NBD1 begins at Asp-665 (Fig. 1*A*). Furthermore, the overlay of resonances in the N-tail spectrum with resonances in the NBD1 spectrum from residues Ser-615–Glu-664 (Fig. 2*B* and see below) indicates that the presence of the folded NBD1 core does not induce folding of the N-tail. Notably, residues Leu-607–Glu-664 in SUR2B are primarily predicted as being disordered (32) by PONDR analysis (58–60). We have also recorded spectra on longer N-tail proteins (Gln-600–Glu-664 and Ser-608–Glu-664). Resonances in the spectra of the N-tail from Ser-615–Glu-664 overlay with resonances in the longer N-tail proteins, indicating that extension of N-tail does not induce folding of these residues. However, NBD1-containing proteins starting at residues Gln-600 or Ser-608 aggregate at the high concentrations required for NMR studies (32), as is often seen when unstructured residues are included in constructs that contain folded domains (61). Thus, for comparison with NBD1 proteins, we are using an N-tail protein beginning at Ser-615.

Phosphorylation of NBD1, NBD1-ΔC, and N-tail is monitored by changes in the chemical shift of the indole HN resonance of Trp-616 (Fig. 3, $W616_{indole}$ *versus* $W616_{indole}$-phospho). The identity of the Trp-616 indole HN resonance in NBD1 and NBD1-ΔC is known from two-dimensional ^{15}N-^{1}H NMR spectra of a deletion mutant of NBD1 in which residues Ser-615–Arg-617 were removed (32). The overlay of the indole HN resonance from Trp-616, the only Trp in the N-terminal tail, in the spectra of NBD1 and the N-tail (Fig. 2) confirms assignment of the Trp-616 indole HN resonance. The combined chemical shift change ($\Delta\delta_{tot}$ of 37 Hz) for the Trp-616 indole HN resonance and its location in a sparsely populated region of the spectrum allow for monitoring of the phosphorylation reaction. Chemical shift changes in the Trp-616 indole HN resonance indicate that it takes ~16 h to completely phosphorylate an NMR sample containing the 200 μM NBD1 at 30 °C (Fig. 2) and ~6 h to completely phosphorylate the 200 μM N-tail at 30 °C. Samples of NBD1-ΔC were also phosphorylated using the same protocol, but to a lower extent. According to peak intensities of the Trp-616 indole HN resonance from the non-phosphorylated and phosphorylated states, NBD1-ΔC is ~85% phosphorylated. We could not achieve uniform phosphorylation of NBD1-ΔC with higher temperatures due to compromised sample stability. Nonetheless, chemical shift changes observed with phosphorylation of NBD1 are also seen with phosphorylation of NBD1-ΔC (see below). Thus, information gleaned from phosphorylation of NBD1-ΔC can be applied to NBD1.

The identity of the phosphorylation sites was determined using mass spectrometry following in-gel trypsin digestion (Fig. 4*A*). Previous studies determined that NBD1 is phosphorylated at the PKA consensus site Thr-632, as well as at another unidentified site, as a peptide comprising residues Cys-628–Ile-639 with a T632A mutation can still be phosphorylated by PKA (24). Our mass spectrometry data comparing non-phosphorylated and phosphorylated forms of NBD1, NBD1-ΔC, and N-tail confirm phosphorylation of Thr-632 and identified the second site as Ser-636. Residues Thr-632 and Ser-636 are located in the N-tail of NBD1 (Fig. 1). No phosphorylation sites were detected in the core of the NBD1. These data are consistent with control NMR phosphorylation experiments that show no chemical shift changes in the spectra of NBD1-ΔN and NBD1-ΔNΔC proteins, which lack Thr-632 and Ser-636.

The phosphorylation site Thr-632 conforms to the PKA consensus site ((R/K)(R/K)X(*p*S/pT)) (62, 63), whereas Ser-636 comprises a non-consensus PKA phosphorylation site (Fig. 4*B*). Phosphorylation of non-canonical sites by PKA has been demonstrated to modulate the function of other proteins (64–66). Furthermore, work with model peptides indicates that PKA can phosphorylate a Ser or Thr residue even if the dibasic motif is located up to eight residues N-terminal to the phosphorylation site, albeit with varying efficiency (67). Thus, the proximity of the two phosphorylation sites in SUR2B NBD1 may allow for the dibasic residues comprising the con-sensus site at Thr-632 to serve in PKA recognition of the non-consensus site Ser-636.

Phosphorylation-dependent Spectral Changes in SUR2B NBD1—In addition to the Trp-616 indole HN group, phosphorylation-dependent chemical shift changes are observed for two additional Trp indole HN and 40 backbone HN resonances in NBD1 (Fig. 5*A*) and for two additional Trp indole resonance and 48 backbone resonances in NBD1-ΔC (Fig. 6*A*). Chemical shift changes are expected for residues close in space to the phosphorylation sites. Phosphorylation of Thr-632 and Ser-636

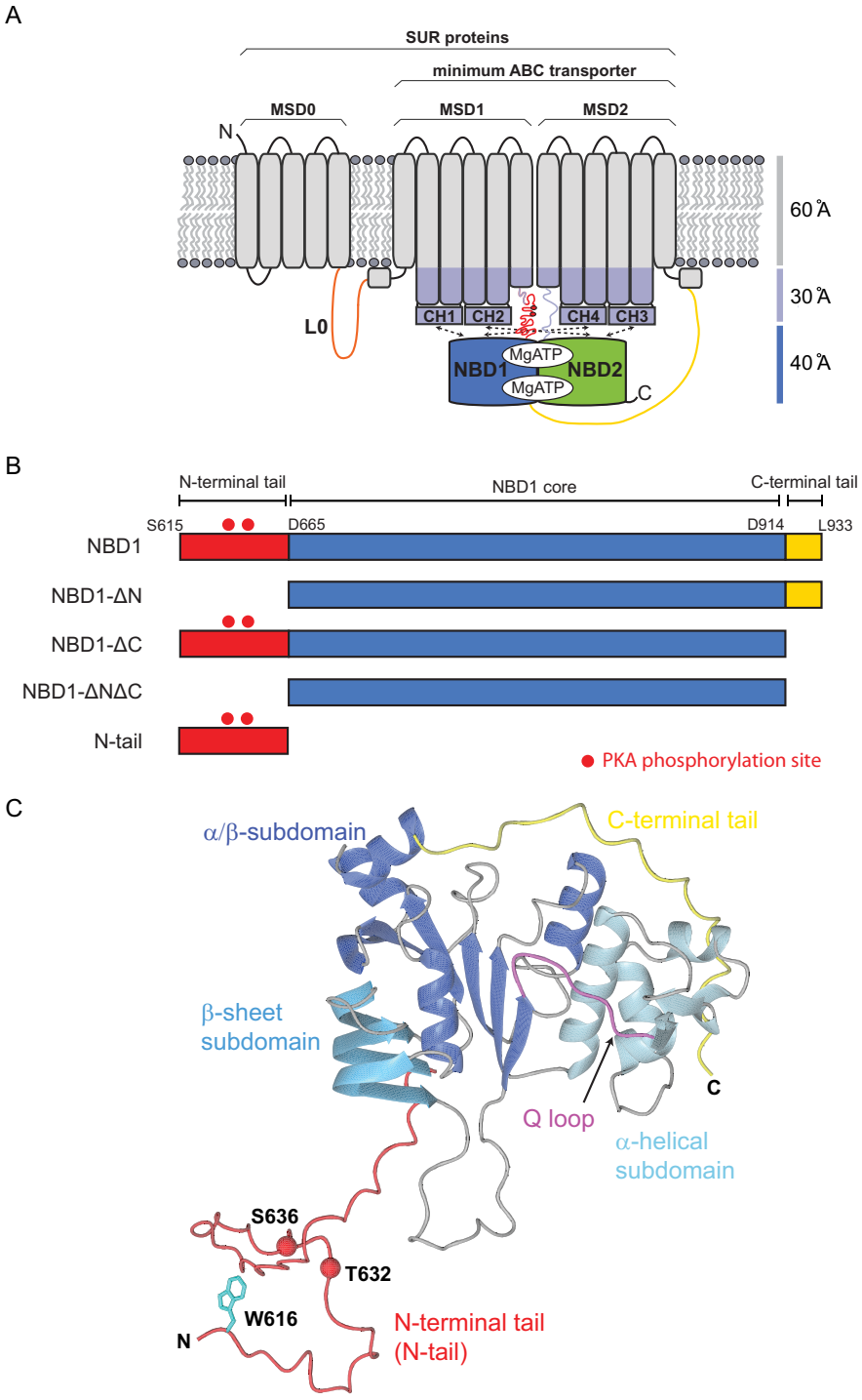

FIGURE 1. **Schematic diagrams of full-length SUR2B and SUR2B NBD1.** *A,* schematic diagram of an SUR protein. The transmembrane helices in each membrane spanning domain (MSD0, MSD1, and MSD2) are shown in *gray*. The L0 linker, shown in *orange*, connects MSD0 to the minimum ABC transporter structure. Cytoplasmic extensions of the transmembrane helices and coupling helices (*CH1*, *CH2*, *CH3*, and *CH4*) in MSD1 and MSD2 are shown in *light purple*. Together, these regions form the intracellular domains. NBD1 and NBD2 are shown in *blue* and *green*, respectively. The N-terminal tail connecting MSD1 to NBD1 is shown in *red*, and the C-terminal tail connecting NBD1 to MSD2 is shown in *yellow*. Phosphorylation sites in the N-terminal tail are indicated as *red circles*. *Scale bars* on the *right* indicate the lengths throughout the protein as determined from homology models of SUR2B based on crystal structures of other ABC transporters (51–54, 56, 57). The length of the lines representing the L0 linker, N-terminal tail, and C-terminal tail were determined assuming that these linkers are completely disordered. Notice that because the intracellular domains are only 30 Å in length, the N-terminal tail is drawn with multiple bends to fit it into the space allocated in the two-dimensional representation. *B,* schematic diagram of NBD1 (residues Ser-615–Leu-933), NBD1-ΔC (residues Ser-615–Asp-914), NBD1-ΔN (residues Asp-665–Leu-933), NBD1-ΔNΔC (residues Asp-665–Asp-914), and N-tail (residues Ser-615–Glu-664). As in *A*, the NBD1 core is in *blue*, the N-terminal extension that is missing in NBD1-ΔN is in *red*, and the C-terminal extension that is missing in NBD1-ΔC is in *yellow*. *C,* schematic ribbon diagram of the homology model of SUR2B NBD1 is based on the crystal structure of MRP1 NBD1 (Protein Data Bank code 2CBZ (95)). The coloring is as in *A* and *B*, with the exception that the different subdomains in the NBD1 core are colored in different shades of *blue*. The α/β subdomain, which contains the MgATP-binding site, is in *dark blue*; the β-sheet subdomain is in *cyan*, and the α-helical subdomain is in *light blue*. The side chain of Trp-616 is shown in *cyan*, and the Q-loop (also known as the γ-phosphate loop) is in *magenta*. The N-terminal tail is shown in an extended conformation because there were no restraints placed on these residues in the modeling. All structure figures were created using MOLMOL (96).

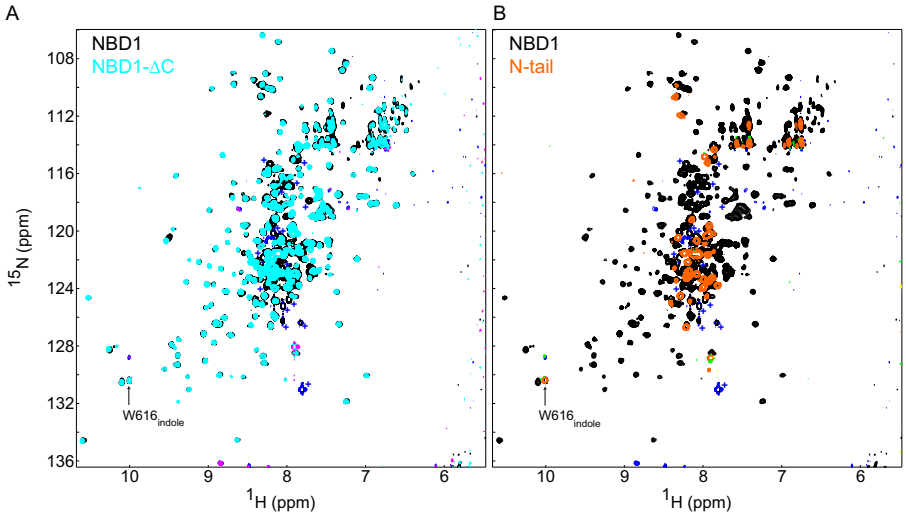

FIGURE 2. **Identification of resonances from the NBD1 core, the N-terminal tail, and the C-terminal tail.** *A,* comparison of two-dimensional ^{15}N-TROSY-HSQC spectra of NBD1 (250 μM) and NBD1-ΔC (220 μM) with 5 mM Mg^{2+} and 5 mM ATP in 20 mM Na^{+} phosphate, pH 7.3, 150 mM NaCl, 2 mM DTT, 2% (v/v) glycerol, 10% (v/v) D_2O at 30 °C at 600 MHz. The spectrum of non-phospho-NBD1 is in the *background* with resonances of backbone nuclei, as well as those from side chain nuclei from Trp, Asn, and Gln residues, shown in *black*. The *blue* resonances are of opposite sign, caused by spectral aliasing, and are possibly from Arg NεHε side chain correlations. The spectrum of NBD1-ΔC is in the *foreground*. The *cyan* and *magenta peaks* in the NBD1-ΔC spectrum correspond to the *black* and *blue resonances*, respectively, in the NBD1 spectrum. *B,* comparison of two-dimensional ^{15}N-TROSY-HSQC spectra of NBD1 and N-tail. The NBD1 spectrum is colored as in *A*. The N-tail spectrum is colored in *orange*. The solution conditions of N-tail are identical to that of NBD1, except that the N-tail buffer lacks MgATP and contains 2 mM tris(2-carboxyethyl)phosphine-HCl in place of DTT.

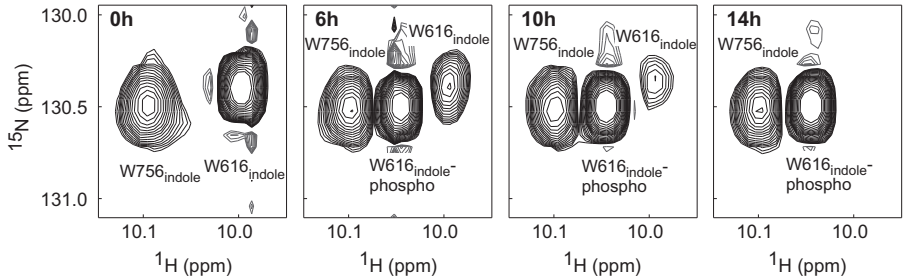

FIGURE 3. **Time course of PKA phosphorylation of SUR2B NBD1.** Only the region of two-dimensional ^{1}H-^{15}N TROSY-HSQC showing two of the Trp indole resonances is displayed. The *most left-hand panel* (0 h) displays the spectrum before addition of PKA. Spectra were recorded every 2 h up to 16 h. An additional spectrum was also recorded after 2 weeks. Selected spectra from the reaction are shown. The Trp indole resonance from residue Trp-616 is used to monitor phosphorylation. The Trp-616 Trp indole resonance is labeled Trp-616$_{indole}$ in the non-phosphorylated state, and it is labeled as Trp-616$_{indole}$-phospho in the phosphorylated state.

introduces two negative charges each into otherwise polar but uncharged side chains, and thus it significantly changes the chemical environment for residues close to Thr-632 and Ser-636. The *cyan circles* in Figs. 5*A* and 6*A* highlight phosphorylation-dependent chemical shift changes common to NBD1 and NBD1-ΔC, and the *magenta squares* highlight phosphorylation-dependent chemical shift changes that are specific to each protein.

Analysis of the NMR spectra indicates that phosphorylation of the N-terminal tail affects both disordered and structured residues in NBD1 and NBD1-ΔC. Of the backbone HN resonances that exhibit chemical shift changes, 6 in NBD1 and 10 in NBD1-ΔC have intense signals and are centered about 8.2 ppm in the ^{1}H dimension (Figs. 5*A* and 6*A*, respectively). Comparison of spectra of NBD1, NBD1-ΔN, NBD1-ΔC, NBD1-ΔNΔC, and N-tail indicates that these intense HN resonances are from the residues in the N-terminal tail (*highlighted* with * in Figs. 5 and 6), as is expected considering the location of the phosphorylation sites, and not the C-terminal tail. Furthermore, the quality of the NBD1-ΔNΔC spectrum indicates that the structural boundaries of the NBD1 core in SUR2B are from residues Asp-665–Asp-914 (Fig. 6*B*). Some of the disordered resonances that exhibit chemical shift changes are seen only with phosphorylation of NBD1-ΔC (Fig. 6*A*, *magenta squares*). However, these resonances may also be present in the spectra of NBD1 and phospho-NBD1 but may be overlapped by the additional disordered residues from the C-terminal tail in NBD1. We cannot assign the remaining disordered resonances that change with phosphorylation to the N-terminal tail due to resonance overlap in this region of the spectrum. The chemical shift change of the indole HN resonance from Trp-616, which is also located in the disordered N-terminal tail (Fig. 1*C*), demonstrates that phosphorylation affects residues far from Thr-632 and Ser-636 in the primary sequence. Chemical shift changes of the Trp-616 indole would not be expected if the N-terminal tail is completely disordered and residues Trp-616, Thr-632, and Ser-636 were independent of one another.

In keeping with the long range effects seen with the Trp-616 indole HN resonance change, phosphorylation of the disordered N-terminal tail also affects multiple structured residues

A

Non-phospho-NBD1

T632-containing peptide

B	B Ions	B+2H	B–NH3	B–H2O	AA	Y Ions	Y+2H	Y–NH3	Y–H2O	Y
1	129.1	65.1	112.1		K	1,364.8	682.9	1,347.7	1,346.8	12
2	266.2	133.6	249.1		H	1,236.7	618.8	1,219.7	1,218.7	11
3	367.2	184.1	350.2	349.2	T	1,099.6	550.3	1,082.6	1,081.6	10
4	424.2	212.6	407.2	406.2	G	998.6	499.8	981.5	980.6	9
5	523.3	262.2	506.3	505.3	V	941.6	471.3	924.5	923.5	8
6	651.4	326.2	634.3	633.3	Q	842.5	421.7	825.5	824.5	7
7	738.4	369.7	721.4	720.4	S	714.4	357.7	697.4	696.4	6
8	866.5	433.7	849.5	848.5	K	627.4	314.2	610.4		5
9	963.5	482.3	946.5	945.5	P	499.3	250.2	482.3		4
10	1,076.6	538.8	1,059.6	1,058.6	I	402.2	201.6	385.2		3
11	1,190.7	595.8	1,173.6	1,172.7	N	289.2	145.1	272.1		2
12	1,364.8	682.9	1,347.7	1,346.8	R	175.1	88.1	158.1		1

phospho-NBD1

pT632-containing peptide

B	B Ions	B+2H	B–NH3	B–H2O	AA	Y Ions	Y+2H	Y–NH3	Y–H2O	Y
1	129.1	65.1	112.1		K	1,444.7	722.9	1,427.7	1,426.7	12
2	266.2	133.6	249.1		H	1,316.6	658.8	1,299.6	1,298.6	11
3	447.2	224.1	430.1	429.2	T+80	1,179.6	590.3	1,162.6	1,161.6	10
4	504.2	252.6	487.2	486.2	G	998.6	499.8	981.5	980.6	9
5	603.3	302.1	586.2	585.3	V	941.6	471.3	924.5	923.5	8
6	731.3	366.2	714.3	713.3	Q	842.5	421.7	825.5	824.5	7
7	818.4	409.7	801.3	800.3	S	714.4	357.7	697.4	696.4	6
8	946.5	473.7	929.4	928.4	K	627.4	314.2	610.4		5
9	1,043.5	522.3	1,026.5	1,025.5	P	499.3	250.2	482.3		4
10	1,156.6	578.8	1,139.6	1,138.6	I	402.2	201.6	385.2		3
11	1,270.6	635.8	1,253.6	1,252.6	N	289.2	145.1	272.1		2
12	1,444.7	722.9	1,427.7	1,426.7	R	175.1	88.1	158.1		1

S636-containing peptide

B	B Ions	B+2H	B–NH3	B–H2O	AA	Y Ions	Y+2H	Y–NH3	Y–H2O	Y
1	138.1	69.5			H	1,236.7	618.8	1,219.7	1,218.7	11
2	239.1	120.1		221.1	T	1,099.6	550.3	1,082.6	1,081.6	10
3	296.1	148.6		278.1	G	998.6	499.8	981.5	980.6	9
4	395.2	198.1		377.2	V	941.6	471.3	924.5	923.5	8
5	523.3	262.1	506.2	505.3	Q	842.5	421.7	825.5	824.5	7
6	610.3	305.7	593.3	592.3	S	714.4	357.7	697.4	696.4	6
7	738.4	369.7	721.4	720.4	K	627.4	314.2	610.4		5
8	835.4	418.2	818.4	817.4	P	499.3	250.2	482.3		4
9	948.5	474.8	931.5	930.5	I	402.2	201.6	385.2		3
10	1,062.6	531.8	1,045.5	1,044.6	N	289.2	145.1	272.1		2
11	1,236.7	618.8	1,219.7	1,218.7	R	175.1	88.1	158.1		1

pS636-containing peptide

B	B Ions	B+2H	B–NH3	B–H2O	AA	Y Ions	Y+2H	Y–NH3	Y–H2O	Y
1	138.1	69.5			H	1,316.6	658.8	1,299.6	1,298.6	11
2	239.1	120.1		221.1	T	1,179.6	590.3	1,162.6	1,161.6	10
3	296.1	148.6		278.1	G	1,078.5	539.8	1,061.5	1,060.5	9
4	395.2	198.1		377.2	V	1,021.5	511.3	1,004.5	1,003.5	8
5	523.3	262.1	506.2	505.3	Q	922.5	461.7	905.4	904.4	7
6	690.3	345.6	673.2	672.3	S+80	794.4	397.7	777.4	776.4	6
7	818.4	409.7	801.3	800.3	K	627.4	314.2	610.4		5
8	915.4	458.2	898.4	897.4	P	499.3	250.2	482.3		4
9	1,028.5	514.7	1,011.5	1,010.5	I	402.2	201.6	385.2		3
10	1,142.5	571.8	1,125.5	1,124.5	N	289.2	145.1	272.1		2
11	1,316.6	658.8	1,299.6	1,298.6	R	175.1	88.1	158.1		1

B

```
615                SWRTGEGTLPFESCKKHTGVQSKPINRKQPGRYHLDNYEQARRLRP
                                   canonical   non-canonical
                                   PKA site    PKA site

661   AETEDVAIKVTNGYFSWGSGLATLSNIDIRIPTGQLTMIVGQVGCGKSSLLLAILGEMQT

721   LEGKVYWNNVNESEPSFEATRSRSRYSVAYAAQKPWLLNATVEENITFGSSFNRQRYKAV

781   TDACSLQPDIDLLPFGDQTEIGERGINLSGGQRQRICVARALYQNTNIVFLDDPFSALDI

841   HLSDHLMQEGILKFLQDDKRTVVLVTHKLQYLTHADWIIAMKDGSVLREGTLKDIQTKDV

901   ELYEHWKTLMNRQDQELEKDMEADQTTLERKTL
```

FIGURE 4. **Mass spectrometry data identify the Thr-632 and Ser-636 phosphorylation sites.** *A,* mass spectrometry data on the nonphospho- and phospho-NBD1. Fragmentation tables for the Thr-632- and Ser-636-containing peptides in non-phospho-NBD1 are shown in the *left panel*. Fragmentation tables for the phosphorylated peptides, the Thr(P)-632- and Ser(P)-636-containing peptides, in phospho-NBD1 are shown in the *right panel*. Values *highlighted* in *pink* correspond to singly-charged B and doubly-charged B ions, and values *highlighted* in *blue* correspond to singly-charged Y and doubly-charged Y ions. The values in *green* correspond to B or Y ions with a loss of ammonia or water. Values corresponding to predicted fragments that are not observed are not highlighted. Fragmentation tables were created with the software Scaffold (Proteome software). *B,* phosphorylation sites in NBD1. The canonical PKA phosphorylation consensus sequence, which contains Thr-632, is in *red boldface type*, and the non-canonical phosphorylation site Ser-636 is shown in *purple boldface type*.

in NBD1 and NBD1-ΔC. Phosphorylation-dependent chemical shift changes in NBD1 are observed for residues throughout the NBD core (Figs. 5*A* and 6*A*). These include residues in the β-sheet subdomain (Ile-691, Leu-721, Tyr-726, and Trp-727), the α-helical subdomain (Thr-767–Gly-769, Arg-776, Tyr-777, Cys-784, and Gly-811), and 27 residues in the α/β subdomain, which contains the MgATP-binding site. Notably, many of the α/β subdomain residues that exhibit chemical shift changes cluster together at or near the interface between the α/β- and α-helical subdomains (Val-748–Ala-751, Gln-824–Thr-826, Phe-830, and Leu-831). Residues in the Q-loop (Gln-753 and Trp-756–Asn-759) also display phosphorylation-dependent chemical shift changes. MgATP binding results in conformational changes in the Q-loop and, along with NBD1/NBD2 dimerization, also alters the relative orientation of α-helical subdomain with the rest of the protein (68–71). Notably, chemical shift changes are also observed for several residues that are located at the predicted NBD1/NBD2 dimer interface (Gln-753, Trp-756, Gly-811, His-841, Glu-904, and His-905). Thus, the phosphorylation-dependent changes of the functional NBD1 residues may be coupled to altered NBD1 activity.

Similar changes are seen upon phosphorylation of NBD1-ΔC. However, the decreased overlap afforded by the nonphospho- and phospho-NBD1-ΔC spectra allow identification of additional residues that exhibit phosphorylation-dependent changes. These include Asn-729 and Val-730, which are located in a loop connecting the β-sheet and α/β subdomains, and Lys-907 located NBD1/NBD2 dimer interface. Phosphorylation also causes chemical shift changes in the indole HN resonances of Trp-727 and Trp-756 in NBD1 (Fig. 5*A*) and of Trp-756 and Trp-906 in NBD1-ΔC (Fig. 6*A*).

Analysis of the homology model of SUR2B NBD1 indicates that phosphorylation affects residues that are up to ~40 Å away

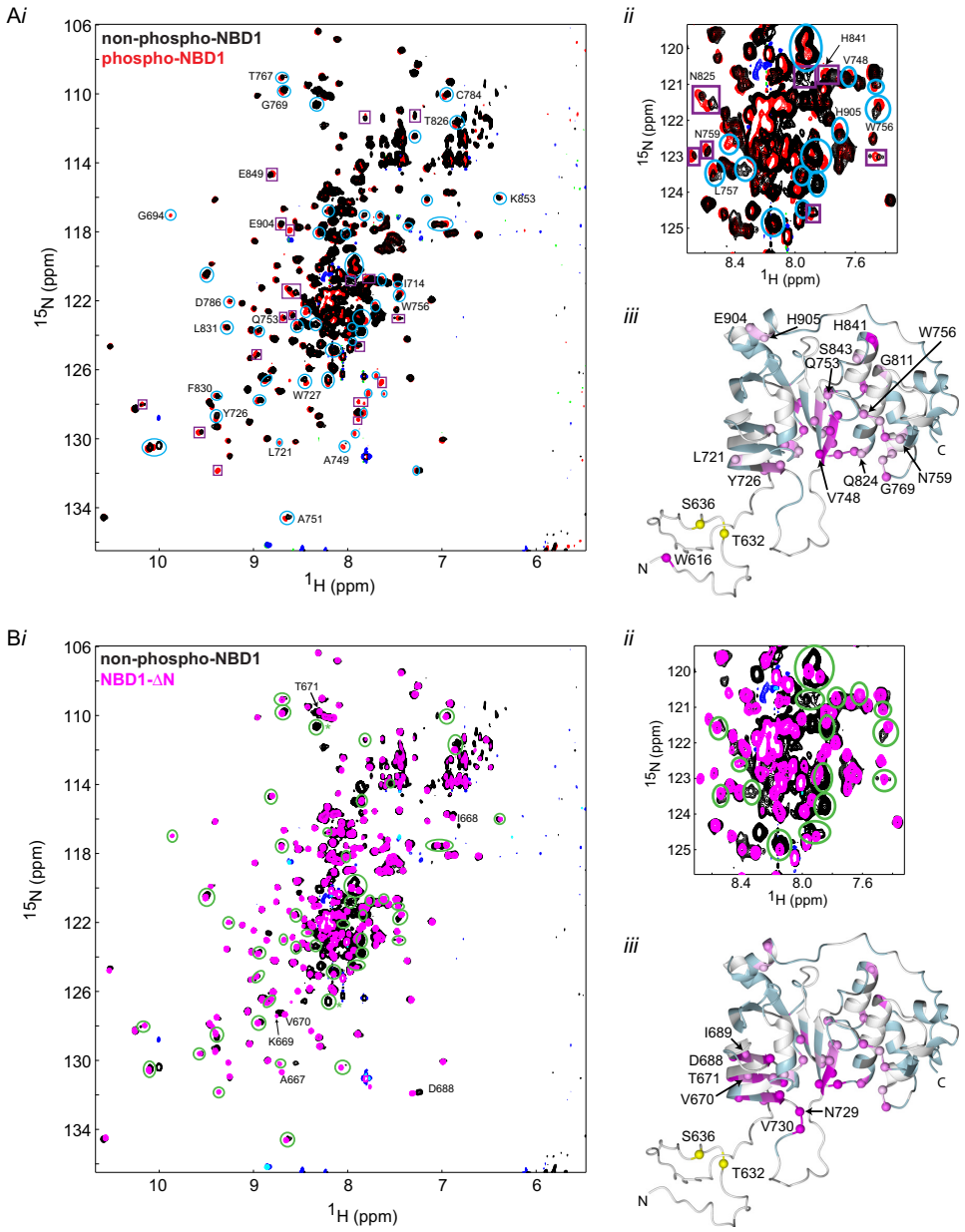

FIGURE 5. **Spectral changes in NBD1 with phosphorylation and removal of the N-terminal tail.** *A, panel i,* comparison of two-dimensional ^{15}N-TROSY-HSQC spectra of non-phospho-NBD1 (250 μM) and phospho-NBD1 (200 μM). The solution conditions for each sample are identical to that described in the legend to Fig. 2. The spectrum of non-phospho-NBD1 is in the *foreground* and is colored as in Fig. 2. The spectrum of phospho-NBD1 is shown in the *background*. The *red* and *green peaks* in the phospho-NBD1 spectrum correspond to the *black* and *blue resonances*, respectively, in the non-phospho-NBD1 spectrum. *A, panel ii,* selected region of the overlaid spectra shown in *A*. Resonances *highlighted* by *cyan circles* highlight phosphorylation-dependent chemical shift changes that also occur in NBD1- ΔC. *Magenta squares* represent chemical shift changes seen with phosphorylation of NBD1 only. Assignment of selected resonances that exhibit phosphorylation-dependent chemical shift changes is shown. *A, panel iii,* chemical shift mapping of phosphorylation-dependent changes to specific residues in NBD1. The *ribbon* diagram is colored *cyan* for residues with resonance assignments, *white* for residues with no resonance assignments, and *gray* for residues that have assignments in NBD1-ΔN but not phospho-NBD1. The location of Pro residues is also indicated in *gray*, as these residues do not give signals in the NH-based NMR experiments, such as the two-dimensional ^{15}N-TROSY-HSQC. Cα atoms of residues that exhibit phosphorylation-dependent chemical shift changes are shown as *spheres* colored from *light pink*, to highlight the smallest changes ($\Delta\delta_{tot}$ = 8–10 Hz), to *magenta* for the largest changes ($\Delta\delta_{tot} \geq$25 Hz). The Cα atoms of Thr-632 and Ser-636 are colored *yellow*. *B, panel i,* comparison of two-dimensional ^{15}N-TROSY-HSQC spectra of non-phospho-NBD1 and NBD1-ΔN (250 μM) The spectrum of non-phospho-NBD1 is shown in the *background* in *black* and *blue*, as in *A*. The spectrum of NBD1-ΔN is in the *foreground*. The *magenta* and *cyan peaks* in the NBD1-ΔN spectrum correspond to the *black* and *blue resonances*, respectively, in the non-phospho-NBD1 spectrum. *B, panel ii,* selected region of the overlaid spectra shown in *A*. *Green circles* highlight resonances that also display chemical shift changes with phosphorylation. Assignment of selected resonances that exhibit chemical shift changes with deletion of the N-terminal tail only are shown. *B, panel iii,* chemical shift mapping of N-terminal tail deletion to specific residues in NBD1. The *ribbon* diagram is colored as in *A*, except that residues colored in *gray* represent residues that have been assigned in spectra of NBD1-ΔN recorded at 800 MHz at 25 °C that cannot be transferred to NBD1-ΔN spectra recorded at 600 MHz at 30 °C. Selected residues that exhibit changes with removal of the N-terminal tail, only, are *highlighted*.

from the end (*i.e.* residue Glu-664) of the N-terminal tail (Figs. 5*A* and 6*A*). One hypothesis for the long range chemical shift changes is that the N-terminal tail possesses residual structure and interacts with multiple regions in the core of NBD1 and that phosphorylation alters the structure of the N-terminal tail and/or its interactions with the NBD core. The interaction of

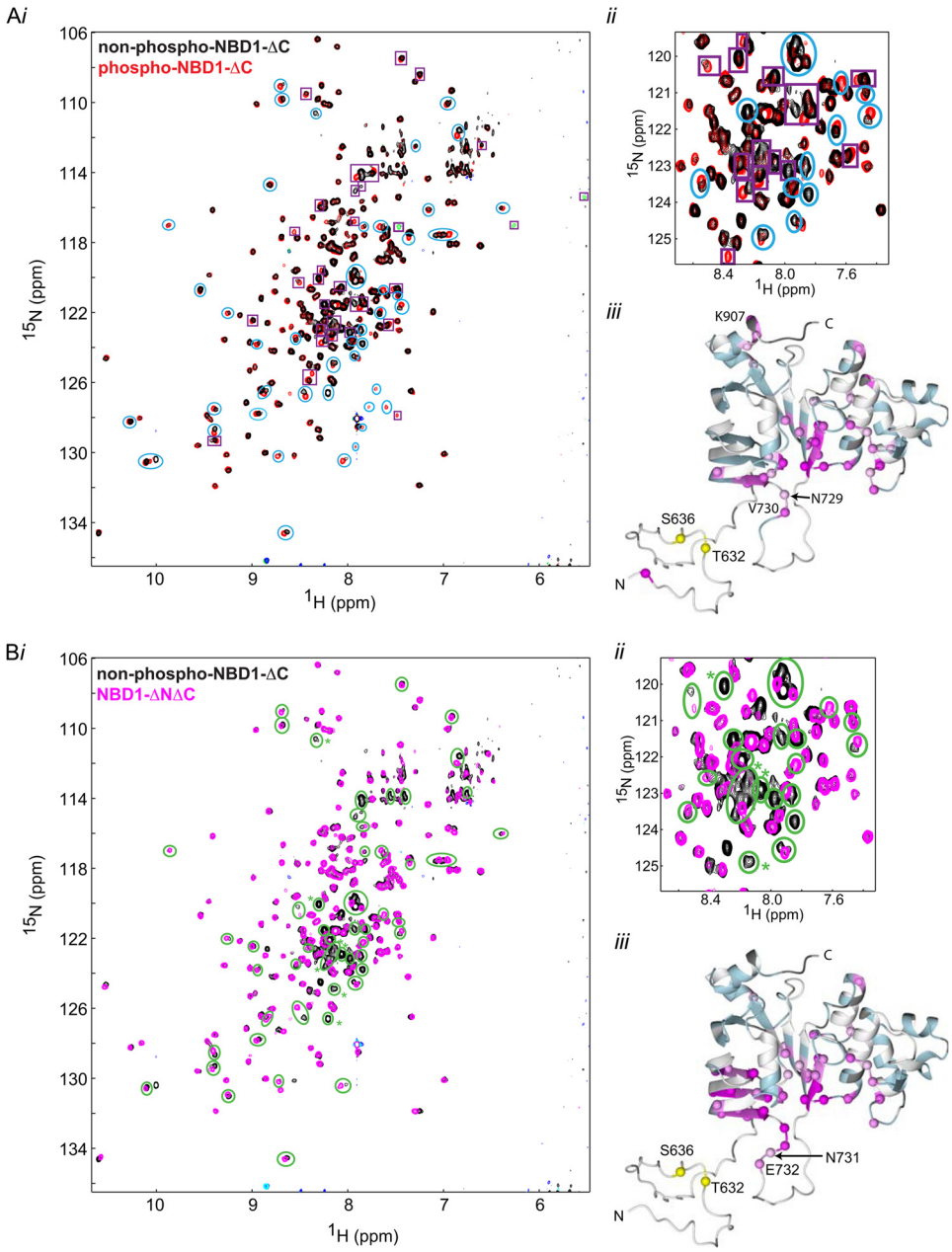

FIGURE 6. **Spectral changes in NBD1-ΔC with phosphorylation and removal of the N-terminal tail.** *A,* two-dimensional ^{15}N-TROSY-HSQC spectra showing phosphorylation-dependent changes in NBD1-ΔC. *A, panel i,* spectrum of non-phospho-NBD1-ΔC (250 μM) is in the *foreground*, and the spectrum of phospho-NBD1-ΔC (80 μM) is in the *background*, with coloring as described for Fig. 5*A*. The solution conditions for each sample are identical to those described in Fig. 5. *A, panel ii,* selected region of the overlaid spectra shown in *A*. *Cyan circles* highlight resonances that also display chemical shift changes with phosphorylation of NBD1. *Magenta squares* highlight resonances that display phosphorylation-dependent chemical shift changes in NBD1-ΔC only. Phosphorylation-dependent chemical shift changes are seen for backbone resonances (*black peaks*) and resonances from NεHε groups in Arg side chains (*green peaks*). *A, panel iii,* chemical shift mapping of phosphorylation-dependent changes to specific residues in NBD1-ΔC. The *ribbon* diagram is colored based on available resonance assignments for phospho-NBD1-ΔC and chemical shift changes. The Cα atoms for selected residues that show phosphorylation-dependent chemical shift changes in NBD1-ΔC, but not NBD1, are *highlighted*. *B, panel i,* comparison of two-dimensional ^{15}N-TROSY-HSQC spectra of non-phospho-NBD1-ΔC and NBD1-ΔNΔC (320 μM) The spectrum of non-phospho-NBD1-ΔC is shown in the background in *black* and *blue*, as in *A*. The spectrum of NBD1-ΔNΔC is in the *foreground*. The *magenta* and *cyan peaks* in the NBD1-ΔNΔC spectrum correspond to the *black* and *blue resonances*, respectively, in the non-phospho-NBD1-ΔC spectrum. *B, panel ii,* selected region of the overlaid spectra shown in *A*. *Green circles* highlight resonances that also display chemical shift changes with phosphorylation. *B, panel iii,* chemical shift mapping of N-terminal tail deletion to specific residues in NBD1-ΔC. Residues are colored based on available resonance assignments for NBD1-ΔNΔC and chemical shift changes. The Cα atoms for selected residues that exhibit chemical shift changes with deletion of the N-terminal tail in NBD1-ΔC, but not NBD1, are *highlighted*.

disordered proteins or disordered residues of a folded protein with multiple binding sites has been observed for many intrinsically disordered proteins (30, 72).

Chemical shift mapping of phosphorylation-dependent changes in NBD1 and NBD1-ΔC is possible because most backbone and Trp indole HN chemical shift assignments of NBD1-ΔN can be transferred to spectra of phospho-NBD1 and phospho-NBD1-ΔC. The remaining backbone resonances (2 in NBD1 and 11 in NBD1-ΔC) that display chemical shift changes are not mapped to specific residues either because they have

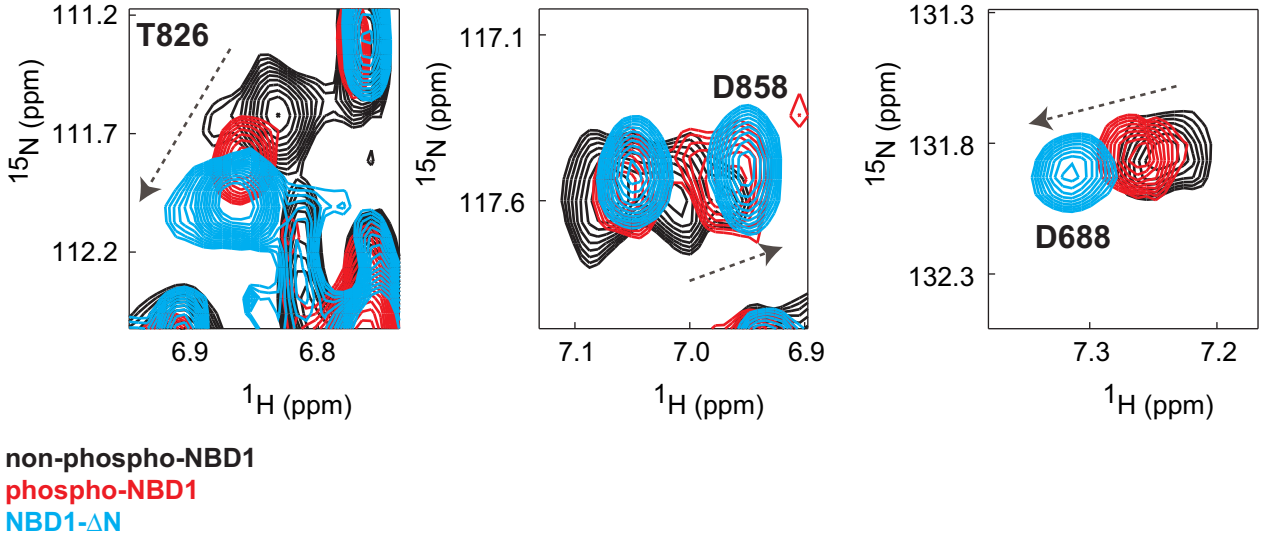

FIGURE 7. **Phosphorylation alters the equilibrium of N-terminal tail interactions.** Selected regions of the spectra of non-phospho-NBD1 (*black*), phospho-NBD1 (*red*), and NBD1-ΔN (*cyan*) are overlaid. *Arrows* highlight the direction of the linear chemical shift changes observed upon phosphorylation of NBD1 and removal of the N-terminal tail.

not been assigned in the spectra of NBD1-ΔN or because assignments could not be transferred from the spectra of NBD1-ΔN to the spectra of phospho-NBD1 and/or phospho-NBD1-ΔC.

Removal of the N-terminal Region Mimics Phosphorylation of NBD1—To determine how phosphorylation alters the conformation of NBD1, we compared spectra of NBD1, phospho-NBD1, and NBD1-ΔN (Fig. 5) as well as NBD1-ΔC, phospho-NBD1-ΔC, and NBD1-ΔNΔC (Fig. 6). Almost every residue in NBD1 and NBD1-ΔC that displays phosphorylation-dependent chemical shift changes also shows chemical shift changes upon removal of the N-terminal tail. Chemical shift changes common to phosphorylation and N-terminal tail removal are *highlighted* by *green circles* in spectra in Figs. 5*B* and 6*B*, respectively, and are also mapped onto the NBD1 model. Additional chemical shift changes in NBD1 and NBD1-ΔC with removal of the N-terminal tail (*e.g.* Ala-667–Thr-671 and Asp-688–Arg-690 resonances in Fig. 5*B*) arise from changing the N-terminal residue in the protein from Ser-615 to Asp-665. This change brings the charged N terminus closer to the NBD1 core and, as expected, causes multiple chemical shift changes for residues in the β-sheet subdomain. In some cases, these chemical shift changes observed with removal of the N-terminal tail were also seen with phosphorylation, but the $\Delta\delta_{tot}$ value calculated for these residues was not statistically significant. Additional differences observed between phosphorylation and removal of the N terminus may result from overlap in spectra of NBD1 and phospho-NBD1 *versus* NBD1 and NBD1-ΔN (and their NBD1-ΔC counterparts), which limits our ability to detect those chemical shift changes. For example, more chemical shift changes are seen with removal of the N-terminal tail compared with phosphorylation for residues in the loop composed of residues Asn-729 to Ser-747.

Notably, a few resonances show linear chemical shift changes (73) when comparing non-phospho-NBD1, phospho-NBD1, and NBD1-ΔN (Fig. 7). Linear chemical shift changes result from fast exchange on the NMR time scale between two distinct states. In the case of SUR2B NBD1, one state consists of the N-terminal tail bound to the NBD1 core, as in non-phospho-NBD1, and the second state has the N-terminal tail fully displaced from the NBD1 core, as in NBD1-ΔN. The intermediate position of phospho-NBD1 resonances indicates that phosphorylation only partly displaces the N-terminal tail from the NBD1 core.

Further differences between non-phospho-NBD1 *versus* phospho-NBD1 and NBD1-ΔN are observed when comparing spectra of the proteins at different temperatures (Fig. 8). Although the spectra of non-phospho-NBD1 show evidence of broadening in backbone and Trp side chain resonances as the temperature is decreased from 30 to 20 °C, spectra of phospho-NBD1 and NBD1-ΔN change very little with temperature. A similar trend is seen for non-phospho-NBD1-ΔC, phospho-NBD1-ΔC, and NBD1-ΔNΔC. For clarity, only a subset of resonances affected by temperature in spectra of non-phospho-NBD1 are highlighted. For example, a number of backbone and Trp indole HN resonances that are observable in spectra of non-phospho-NBD1 at 30 °C (Fig. 8, *solid cyan circles*) are missing in the spectra of non-phospho-NBD1 at 25 °C and/or 20 °C (Fig. 8, *dashed cyan circles* highlight the position of these missing resonances). Notably, some of the non-phospho-NBD1 resonances that completely disappear at 25 °C and/or 20 °C have strong intensities at 30 °C. In contrast, most of these resonances are observable in the spectra of phospho-NBD1 at lower temperatures, and all are observable in NBD1-ΔN in spectra recorded at 25 and 20 °C. Furthermore, phosphorylation of NBD1 and removal of the N-terminal tail from NBD1 results in the appearance of additional peaks (Fig. 8, *magenta circles*). These resonances are likely also present in the spectra of non-phospho-NBD1, but their low intensities do not allow them to be unambiguously distinguished from background noise.

The temperature-induced broadening of non-phospho-NBD1 is reversible, and we have already determined that NMR samples of non-phospho-NBD1 at 250 μM concentration are monomeric (44). Thus, we do not attribute the broadening to

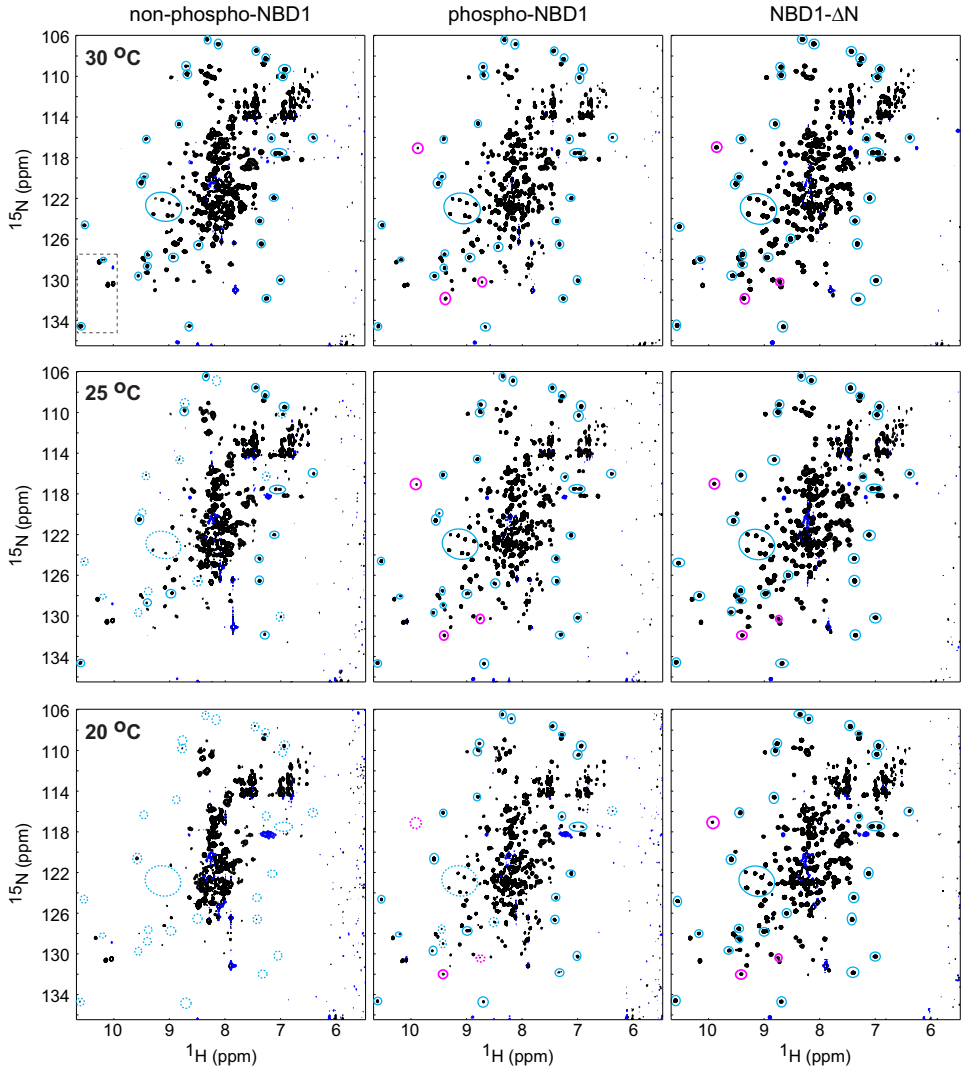

FIGURE 8. **Temperature-dependent changes in spectra of non-phospho-NBD1, phospho-NBD1, and NBD1-ΔN indicate that displacement of the N-terminal tail reduces broadening of resonances from the NBD1 core.** Two-dimensional ^{1}H-^{15}N TROSY-HSQC spectra for each sample were recorded at temperatures of 30 °C (*top panels*), 25 °C (*middle panels*), and 20 °C (*bottom panels*). Backbone HN resonances as well as side chain HN resonances from Trp, Asn, and Gln residues are in *black*. Resonances from Arg NεHε groups are in *blue*. *Solid cyan circles* in all panels highlight backbone and Trp indole HN resonances that are seen in spectra of non-phospho-NBD1 at 30 °C but that experience broadening in spectra of the non-phospho-NBD1 at 25 and 20 °C. *Dashed cyan circles* indicate the positions of the resonances that are broadened in spectra of non-phospho-NBD1 at the lower temperatures. A *gray dotted box* in the spectrum of non-phospho-NBD1 at 30 °C (*upper left*) highlights the Trp indole HN resonances. *Solid magenta circles* highlight backbone resonances that appear in spectra of phospho-NBD1 and NBD1-ΔN. The *dashed magenta circles* highlight the positions of these resonances in spectra of phospho-NBD1 at 20 °C.

NBD1 dimerization or aggregation. Because broadening in NMR spectra can arise from microsecond to millisecond time scale protein motions, these temperature-dependent spectral changes imply differences in NBD1 dynamics, possibly caused by differential interactions of the N-terminal tail with the NBD1 core in the different proteins. In fact, many of the non-phospho-NBD1 resonances that experience temperature-induced broadening also exhibit chemical shift changes with phosphorylation and removal of the N-terminal tail. These include residues in the β-sheet subdomain (Ile-691, Tyr-726, and Trp-727), the ATP binding α/β subdomain (Gly-694, Leu-696, Ile-714, Ala-751, Trp-756, Leu-758, Phe-830, Leu-31, Lys-859, and Asp-876), and the α-helical subdomain (Thr-767, Gly-769, Tyr-777, and Cys-784). Interactions of the N-terminal tail in non-phospho-NBD1 result in multiple NBD1 core residues experiencing μs-ms motions, leading to overall broadening of the spectra. These microsecond-millisecond motions are quenched by the limited interactions of the phosphorylated N-terminal tail and NBD1 core, resulting in reduced broadening in the spectra of phospho-NBD1. The absence of the N-terminal tail binding to the NBD1 core in NBD1-ΔN eliminates broadening in spectra of NBD1-ΔN.

Disruption of the N-terminal tail interactions with the NBD1 core by phosphorylation of Thr-632 and Ser-636 would lead to a less compact protein. To test this model, we measured the hydrodynamic radius of non-phospho- and phospho-NBD1 using dynamic light scattering (Fig. 9). Phosphorylation of Thr-632 and Ser-636 increased the hydrodynamic radius of NBD1 by ~20% from 3.07 ± 0.06 to 3.66 ± 0.07 nm, consistent with our hypothesis. For comparison, NBD1-ΔN has a hydrodynamic radius of 2.35 ± 0.07 nm. The hydrodynamic radius of NBD1-ΔN (30 kDa) is slightly smaller than the hydrodynamic

radius of ovalbumin (45 kDa) of 2.81 ± 0.01 nm. Together, the NMR and the light scattering data suggest that phosphorylation of Thr-632 and Ser-636 disrupts interactions of the N-terminal segment with the core of NBD1.

Phosphorylation Increases the Nucleotide Binding Affinity of NBD1—PKA phosphorylation of SUR2B at NBD1 and NBD2 results in increased K_{ATP} channel activity (24, 26). Because K_{ATP} channel gating is also activated by MgATP binding and hydrolysis at the NBDs, we sought to determine whether phosphorylation alters the nucleotide binding properties of NBD1. We used a fluorescently labeled ATP analogue, TNP-ATP, to probe binding of nucleotide to NBD1 (33, 44). TNP-ATP exhibits very low fluorescence in the absence of NBD1. Addition of increasing amounts of non-phosphorylated NBD1, phosphorylated NBD1, and NBD1-ΔN resulted in a concentration-dependent and saturable increase in TNP-ATP fluorescence (Fig. 10*A*). Fitting of the binding curves reveals a K_d value of 8.4 ± 1.1 μM for the interaction of non-phospho-NBD1 with TNP-ATP, as measured previously (33, 44). In comparison, there is a modest increase in the nucleotide binding affinity for phospho-NBD1 (K_d 6.3 ± 0.2 μM) and a 2-fold increase in the nucleotide binding affinity of NBD1-ΔN (K_d 4.4 ± 0.7 μM). Mg^{2+} was required for these experiments, as no nucleotide binding could be detected without Mg^{2+}, as assessed by TNP-ATP fluorescence binding experiments and NMR titrations with ATP. Note that NBD1 samples for these Mg^{2+}-free studies were dialyzed against a buffer lacking Mg^{2+} and containing Chelex 100 resin to remove any residual metals.

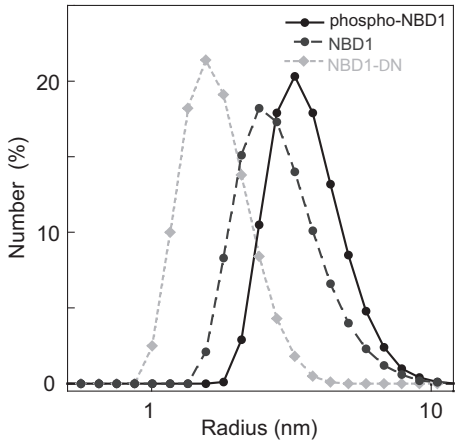

FIGURE 9. **Phosphorylation increases the size of NBD1.** Dynamic light scattering profiles of non-phospho-NBD1 (*gray dashed line*), phospho-NBD1 (*solid black line*), and NBD1-ΔN (*light gray dotted line*) are shown. The frequency distribution of particles at the given size (hydrodynamic radius) is shown for each protein. The fit of the profiles gives a hydrodynamic radius of 3.07 ± 0.06 nm for non-phospho-NBD1, 3.66 ± 0.07 nm for phospho-NBD1, and 2.35 ± 0.07 nm for NBD1-ΔN. Values are reported as averages of three measurements ± 1 S.D.

The intermediate increase in the MgATP binding affinity of phospho-NBD1 is consistent with a model in which phosphorylation of Thr-632 and Ser-636 disrupt interactions of the N-terminal region with the NBD1 core to partly expose the ATP-binding site, with removal of these residues in NBD1-ΔN fully exposing the ATP-binding site. The increased nucleotide binding observed for the isolated and monomeric phospho-NBD1 and NBD1 in which the N-terminal tail is completely displaced from binding the protein core (NBD1-ΔN) likely has a greater effect in the intact channel, which contains four SUR2B proteins. Increased MgATP binding at NBD1 will likely also increase binding of NBD1 and NBD2, which ultimately increases K_{ATP} channel gating (74).

We used intrinsic tryptophan fluorescence to monitor thermal unfolding of the NBD1 proteins (Fig. 10*B*). In the absence of MgATP, phospho-NBD1 and NBD1-ΔN have melting profiles and melting temperatures (T_m ~30 °C) that are similar to that previously seen for NBD1 (33). However, in the presence of MgATP, the proteins have different thermal stabilities. MgATP

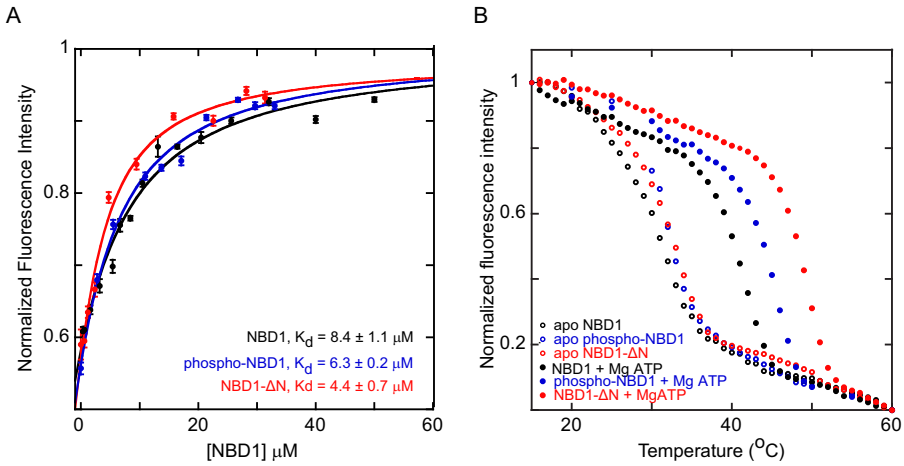

FIGURE 10. **Changes in nucleotide binding with phosphorylation and removal of the N-terminal tail.** *A,* TNP-ATP binding to non-phospho-NBD1, phospho-NBD1, and NBD1-ΔN. The increasing fluorescence of TNP-ATP is shown as *solid circles* in *black, blue*, or *red* for non-phospho-NBD1, phospho-NBD1, and NBD1-ΔN, respectively. *Error bars* show the error in each point from three fluorescence measurements. *Solid lines* displays the fit of the TNP-ATP titration data, assuming a 1:1 complex for the NBD1/nucleotide interaction (46, 47), as described under "Experimental Procedures." The K_d values for binding to TNP-ATP are 8.4 ± 1.1 μM for non-phospho-NBD1, 6.3 ± 0.2 μM for phospho-NBD1, and 4.4 ± 0.7 μM for NBD1-ΔN. *B,* MgATP binding increases in the thermodynamic stability of non-phospho-NBD1 (*black*), phospho-NBD1 (*blue*), and NBD1-ΔN (*red*). Temperature denaturation studies were performed on 2 μM protein samples in a 1-cm cuvette. Data from temperature denaturation of the NBD proteins in the absence and presence of 2 mM MgATP are shown as *open circles* and *filled circles*, respectively. In the absence of MgATP, the T_m value was similar for all proteins (non-phospho-NBD1, 27.7 ± 1.2 °C; phospho-NBD1, 29.7 ± 1.5 °C; NBD1-ΔN, 30.0 ± 1.0 °C). In the presence of 2 mM MgATP, the T_m values are 42.3 ± 0.6 °C for non-phospho-NBD1, 44.7 ± 0.6 °C for phospho-NBD1, and 48.3 ± 0.6 °C for NBD1-ΔN. The K_d values and T_m values are reported as averages of three measurements ± 1 S.D.

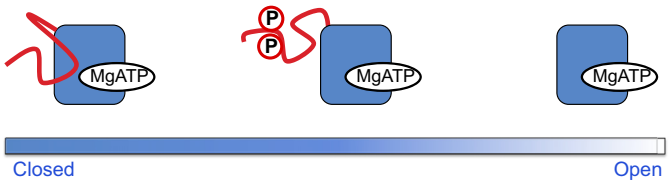

FIGURE 11. **Structural model for effect of phosphorylation of Thr-632 and Ser-636 on interactions of the N-terminal segment with the NBD1 core.** The NBD1 core is shown as a rounded *blue square*, and the N-terminal tail that contains Thr-632 and Ser-636 is shown as a *red line* with phosphorylation indicated by *open red circles* labeled with a *P* as applicable. Different interactions of the N-terminal tail with NBD1 are displayed schematically on a gradient from a "closed state," in which the N-terminal tail is bound to the NBD1 core, to an "open state," where the N-terminal tail is removed and cannot bind the NBD1 core. Phosphorylation of the N-terminal tail results in an intermediate state in which the N-terminal tail makes limited interactions with the NBD core.

leads to a substantial stabilization of all NBD1 samples, with NBD1-ΔN exhibiting the greatest increase in T_m values (T_m = 48 °C), followed by phospho-NBD1 (T_m = 45 °C) and then non-phospho-NBD1 (T_m = 42 °C). This trend in T_m values for the different samples is likely a reflection of the difference in nucleotide binding affinity for the different proteins. ATPase activity of the different NBD1 proteins was measured, as done previously, and was found to be very low (<4.0 nmol of P_i/mg of protein/min) (75, 76), likely because NBD2 was not present.

Discussion

Our NMR studies demonstrate that phosphorylation of Thr-632 and Ser-636 affects residues in the disordered N-terminal tail and the structured NBD1 core. Residue Thr-632 corresponds to a canonical PKA phosphorylation site that is conserved among species, and residue Ser-636 is a variable non-canonical PKA phosphorylation site. Residue Ser-636 in rat and murine SUR2B corresponds to a Pro residue (Pro-639) in human SUR2B, which would promote alternative conformations of the N-terminal tail (77, 78). Furthermore, Pro-639 is part of exon 14 (residues Gln-638–Lys-673) that is missing in a naturally occurring splice isoform, known as human SUR2C (79), which further illustrates the regulatory nature of the N-terminal tail. Our NMR data showing that removal of the N-terminal tail mimics phosphorylation of NBD1 suggest that phosphorylation of Thr-632 and Ser-636 disrupts some of the transient interactions of the N-terminal tail with NBD1, with complete disruption achieved by removal of the N-terminal tail in NBD1-ΔN (Fig. 11). Chemical shift mapping indicates that these transient interactions occur with residues that exhibit conformational changes with MgATP binding, such as residues in the Q-loop and at the interface between the α/β and α-helical subdomains (68–71). The more "open" state of NBD1 achieved by phosphorylation and N-terminal tail deletion would result in increased exposure of the MgATP-binding site, thereby explaining the increased nucleotide binding affinity of phospho-NBD1 and NBD1-ΔN. Chemical shift mapping also indicates that transient interactions occur with NBD1 residues that bind NBD2. Phosphorylation promotes stabilization of NBD1 into a conformation that allows NBD1 to make productive interactions (80), such as with MgATP and/or NBD2, leading to increased K_{ATP} channel opening (12). Thus, the model (Fig. 11) is consistent with the demonstrated phosphorylation-mediated activation of K_{ATP} channels (24, 27). Because SUR2B NBD2 is also phosphorylated, additional studies using NBD2 are necessary. Furthermore, phosphorylation of the NBDs may affect their interactions with other regions of SUR2B, such as the coupling helices, and/or the Kir6.2 channel pore. Therefore, a full understanding of the molecular basis of the mechanism by which multisite phosphorylation regulates K_{ATP} channels will require additional studies to address these questions. Notably, phosphorylation of SUR1 NBD2 also regulates K_{ATP} channel gating (20, 21), suggesting that SUR subunit phosphorylation is a common regulatory mechanism to control K_{ATP} channel gating.

Phosphorylation has been observed for many ABC transporters across all subfamilies, which implies that phosphorylation is a general mechanism for regulating ABC transporter function. ABC transporters are phosphorylated at specific sites in the NBDs and/or in the NBD1-MSD2 linker by various kinases, with the effects of phosphorylation depending on the specific site phosphorylated (81). For example, phosphorylation of ABCA1 at NBD2 is required for full cholesterol transport activity, whereas phosphorylation of the NBD1-MSD2 linker affects protein stability (81–83). ABCB1, which is also known as P-glycoprotein and is associated with multidrug resistance in cancers (84), is also phosphorylated at a number of sites in the NBD1-MSD2 linker by PKA, protein kinase C, and casein kinase 2 (81). PKC phosphorylation increases the ATPase activity of ABCB1 and regulates efflux of anions.

The best characterized ABC protein in terms of phosphorylation is CFTR. Like the SUR proteins, CFTR is a member of the C-subfamily of ABC transporters (5). CFTR is phosphorylated by PKA and PKC at multiple sites in the disordered R region, which links NBD1 to MSD2, and by PKA at one site in the regulatory insert located within NBD1 (85–88). As with SUR2B, phosphorylation of CFTR disrupts transient interactions of the regulatory insert and R region with the NBD1 core (29, 31) to promote a more open CFTR NBD1 conformation (31, 89, 90), which then permits binding of NBD1 with coupling helix 1 (31). Furthermore, as with SUR2B, phosphorylation of CFTR leads to increased MgATP binding and hydrolysis, and subsequent channel activation (28, 48).

Studies of CFTR highlight additional functional consequences of phosphorylation, which may also be relevant for SUR2B. There are differences in the conformation of phosphorylated CFTR with the severe cystic fibrosis-causing mutation ΔF508 (31, 91), which partly explain the molecular defects of mutant CFTR compared with the wild type protein (91–94). Furthermore, deletion of the regulatory insert, which mimics phosphorylation (31), increases the response of mutant CFTR to small molecule correctors (91). Phosphorylation also disrupts interactions of the R region with NBD2, but it enhances interactions of the R region with the C terminus of CFTR and the accessory proteins STAS (sulfate transporters and anti-sigma factor) and 14-3-3 (30). As observed for CFTR, phosphorylated SUR NBDs bearing disease-causing mutations may also possess a different conformation from phosphorylated wild type NBDs. In addition, phosphorylation may affect interactions of the SUR2B NBDs with other proteins, such as the Kir6.2 pore, or with therapeutics, such as pinacidil which binds NBD1

(44). Thus, data presented here on the conformation of wild type SUR2B NBD1 provide a platform to address these additional questions.

Author Contributions—E. D. A. generated all non-phospho-NBD1, phospho-NBD1, and NBD1-ΔN samples and conducted the nucleotide binding and dynamic light scattering experiments. E. D. A. and J. P. L.-A. recorded NMR data on non-phospho-NBD1, phospho-NBD1, and NBD1-ΔN samples. C. P. A. generated the non-phospho-NBD1-ΔC, phospho-NBD1-ΔC, and NBD1-ΔNΔC samples and recorded all NMR spectra of these proteins. C. R. S. generated the N-tail samples and together with E. D. A. recorded NMR spectra of these proteins. M. S. generated initial NBD1-ΔN proteins and performed the initial feasibility studies. V. K. and E. D. A. analyzed the NMR data. Figures were generated by V. K. and E. D. A. The manuscript was written by V. K., with contributions from E. D. A., and edited by V. K., E. D. A., and C. P. A.

Acknowledgments—We thank John L. Rubinstein for critically reading the manuscript and R. Scott Prosser for useful discussions.

References

1. Seino, S., and Miki, T. (2003) Physiological and pathophysiological roles of ATP-sensitive K^+ channels. *Prog. Biophys. Mol. Biol.* **81,** 133–176
2. Nichols, C. G. (2006) K_{ATP} channels as molecular sensors of cellular metabolism. *Nature* **440,** 470–476
3. Proks, P., Antcliff, J. F., Lippiat, J., Gloyn, A. L., Hattersley, A. T., and Ashcroft, F. M. (2004) Molecular basis of Kir6.2 mutations associated with neonatal diabetes or neonatal diabetes plus neurological features. *Proc. Natl. Acad. Sci. U.S.A.* **101,** 17539–17544
4. Mikhailov, M. V., Campbell, J. D., de Wet, H., Shimomura, K., Zadek, B., Collins, R. F., Sansom, M. S., Ford, R. C., and Ashcroft, F. M. (2005) 3-D structural and functional characterization of the purified K_{ATP} channel complex Kir6.2-SUR1. *EMBO J.* **24,** 4166–4175
5. Dean, M., Rzhetsky, A., and Allikmets, R. (2001) The human ATP-binding cassette (ABC) transporter superfamily. *Genome Res.* **11,** 1156–1166
6. Higgins, C. F., and Linton, K. J. (2004) The ATP switch model for ABC transporters. *Nat. Struct. Mol. Biol.* **11,** 918–926
7. Babenko, A. P., and Bryan, J. (2002) SUR-dependent modulation of K_{ATP} channels by an N-terminal KIR6.2 peptide. Defining intersubunit gating interactions. *J. Biol. Chem.* **277,** 43997–44004
8. Boabenko, A. P., and Bryan, J. (2003) Sur domains that associate with and gate K_{ATP} pores define a novel gatekeeper. *J. Biol. Chem.* **278,** 41577–41580
9. Bryan, J., Vila-Carriles, W. H., Zhao, G., Babenko, A. P., and Aguilar-Bryan, L. (2004) Toward linking structure with function in ATP-sensitive K^+ channels. *Diabetes* **53,** S104–S112
10. Fang, K., Csanády, L., and Chan, K. W. (2006) The N-terminal transmembrane domain (TMD0) and a cytosolic linker (L0) of sulphonylurea receptor define the unique intrinsic gating of K_{ATP} channels. *J. Physiol.* **576,** 379–389
11. Zingman, L. V., Alekseev, A. E., Bienengraeber, M., Hodgson, D., Karger, A. B., Dzeja, P. P., and Terzic, A. (2001) Signaling in channel/enzyme multimers: ATPase transitions in SUR module gate ATP-sensitive K^+ conductance. *Neuron* **31,** 233–245
12. Ueda, K., Komine, J., Matsuo, M., Seino, S., and Amachi, T. (1999) Cooperative binding of ATP and MgADP in the sulfonylurea receptor is modulated by glibenclamide. *Proc. Natl. Acad. Sci. U.S.A.* **96,** 1268–1272
13. Flanagan, S. E., Clauin, S., Bellanné-Chantelot, C., de Lonlay, P., Harries, L. W., Gloyn, A. L., and Ellard, S. (2009) Update of mutations in the genes encoding the pancreatic β-cell K(ATP) channel subunits Kir6.2 (KCNJ11) and sulfonylurea receptor 1 (ABCC8) in diabetes mellitus and hyperinsulinism. *Hum. Mutat.* **30,** 170–180
14. Bienengraeber, M., Olson, T. M., Selivanov, V. A., Kathmann, E. C., O'Cochlain, F., Gao, F., Karger, A. B., Ballew, J. D., Hodgson, D. M., Zingman, L. V., Pang, Y. P., Alekseev, A. E., and Terzic, A. (2004) ABCC9 mutations identified in human dilated cardiomyopathy disrupt catalytic K_{ATP} channel gating. *Nat. Genet.* **36,** 382–387
15. Minoretti, P., Falcone, C., Aldeghi, A., Olivieri, V., Mori, F., Emanuele, E., Calcagnino, M., and Geroldi, D. (2006) A novel Val734Ile variant in the ABCC9 gene associated with myocardial infarction. *Clin. Chim. Acta* **370,** 124–128
16. Olson, T. M., Alekseev, A. E., Moreau, C., Liu, X. K., Zingman, L. V., Miki, T., Seino, S., Asirvatham, S. J., Jahangir, A., and Terzic, A. (2007) K_{ATP} channel mutation confers risk for vein of Marshall adrenergic atrial fibrillation. *Nat. Clin. Pract. Cardiovasc. Med.* **4,** 110–116
17. Smith, K. J., Chadburn, A. J., Adomaviciene, A., Minoretti, P., Vignali, L., Emanuele, E., and Tammaro, P. (2013) Coronary spasm and acute myocardial infarction due to a mutation (V734I) in the nucleotide binding domain 1 of ABCC9. *Int. J. Cardiol.* **168,** 3506–3513
18. Hu, D., Barajas-Martínez, H., Terzic, A., Park, S., Pfeiffer, R., Burashnikov, E., Wu, Y., Borggrefe, M., Veltmann, C., Schimpf, R., Cai, J. J., Nam, G. B., Deshmukh, P., Scheinman, M., Preminger, M., *et al.* (2014) ABCC9 is a novel Brugada and early repolarization syndrome susceptibility gene. *Int. J. Cardiol.* **171,** 431–442
19. Arakel, E. C., Brandenburg, S., Uchida, K., Zhang, H., Lin, Y. W., Kohl, T., Schrul, B., Sulkin, M. S., Efimov, I. R., Nichols, C. G., Lehnart, S. E., and Schwappach, B. (2014) Tuning the electrical properties of the heart by differential trafficking of K_{ATP} ion channel complexes. *J. Cell Sci.* **127,** 2106–2119
20. Béguin, P., Nagashima, K., Nishimura, M., Gonoi, T., and Seino, S. (1999) PKA-mediated phosphorylation of the human K(ATP) channel: separate roles of Kir6.2 and SUR1 subunit phosphorylation. *EMBO J.* **18,** 4722–4732
21. Light, P. E., Manning, Fox J. E., Riedel, M. J., and Wheeler, M. B. (2002) Glucagon-like peptide-1 inhibits pancreatic ATP-sensitive potassium channels via a protein kinase A- and ADP-dependent mechanism. *Mol. Endocrinol.* **16,** 2135–2144
22. Lin, Y. F., and Chai, Y. (2008) Functional modulation of the ATP-sensitive potassium channel by extracellular signal-regulated kinase-mediated phosphorylation. *Neuroscience* **152,** 371–380
23. Lin, Y. F., Jan, Y. N., and Jan, L. Y. (2000) Regulation of ATP-sensitive potassium channel function by protein kinase A-mediated phosphorylation in transfected HEK293 cells. *EMBO J.* **19,** 942–955
24. Quinn, K. V., Giblin, J. P., and Tinker, A. (2004) Multisite phosphorylation mechanism for protein kinase A activation of the smooth muscle ATP-sensitive K^+ channel. *Circ. Res.* **94,** 1359–1366
25. Ribalet, B., John, S. A., and Weiss, J. N. (2000) Regulation of cloned ATP-sensitive K channels by phosphorylation, MgADP, and phosphatidylinositol bisphosphate (PIP(2)): a study of channel rundown and reactivation. *J. Gen. Physiol.* **116,** 391–410
26. Shi, Y., Chen, X., Wu, Z., Shi, W., Yang, Y., Cui, N., Jiang, C., and Harrison, R. W. (2008) cAMP-dependent protein kinase phosphorylation produces interdomain movement in SUR2B leading to activation of the vascular K_{ATP} channel. *J. Biol. Chem.* **283,** 7523–7530
27. Shi, Y., Wu, Z., Cui, N., Shi, W., Yang, Y., Zhang, X., Rojas, A., Ha, B. T., and Jiang, C. (2007) PKA phosphorylation of SUR2B subunit underscores vascular K_{ATP} channel activation by β-adrenergic receptors. *Am. J. Physiol. Regul. Integr. Comp. Physiol.* **293,** R1205–R1214
28. Li, C., Ramjeesingh, M., Wang, W., Garami, E., Hewryk, M., Lee, D., Rommens, J. M., Galley, K., and Bear, C. E. (1996) ATPase activity of the cystic fibrosis transmembrane conductance regulator. *J. Biol. Chem.* **271,** 28463–28468
29. Baker, J. M., Hudson, R. P., Kanelis, V., Choy, W. Y., Thibodeau, P. H., Thomas, P. J., and Forman-Kay, J. D. (2007) CFTR regulatory region interacts with NBD1 predominantly via multiple transient helices. *Nat. Struct. Mol. Biol.* **14,** 738–745
30. Bozoky, Z., Krzeminski, M., Muhandiram, R., Birtley, J. R., Al-Zahrani, A., Thomas, P. J., Frizzell, R. A., Ford, R. C., and Forman-Kay, J. D. (2013) Regulatory R region of the CFTR chloride channel is a dynamic integrator of phospho-dependent intra- and intermolecular interactions. *Proc. Natl. Acad. Sci. U.S.A.* **110,** E4427–E4436

31. Kanelis, V., Hudson, R. P., Thibodeau, P. H., Thomas, P. J., and Forman-Kay, J. D. (2010) NMR evidence for differential phosphorylation-dependent interactions in WT and ΔF508 CFTR. *EMBO J.* **29,** 263–277
32. de Araujo, E. D., Ikeda, L. K., Tzvetkova, S., and Kanelis, V. (2011) The first nucleotide binding domain of the sulfonylurea receptor 2A contains regulatory elements and is folded and functions as an independent module. *Biochemistry* **50,** 6655–6666
33. de Araujo, E. D., and Kanelis, V. (2014) Successful development and use of a thermodynamic stability screen for optimizing the yield of nucleotide binding domains. *Protein Expr. Purif.* **103,** 38–47
34. Pervushin, K., Riek, R., Wider, G., and Wüthrich, K. (1997) Attenuated T2 relaxation by mutual cancellation of dipole-dipole coupling and chemical shift anisotropy indicates an avenue to NMR structures of very large biological macromolecules in solution. *Proc. Natl. Acad. Sci. U.S.A.* **94,** 12366–12371
35. Wishart, D. S., Bigam, C. G., Yao, J., Abildgaard, F., Dyson, H. J., Oldfield, E., Markley, J. L., and Sykes, B. D. (1995) 1H, 13C and 15N chemical shift referencing in biomolecular NMR. *J. Biomol. NMR* **6,** 135–140
36. Delaglio, F., Grzesiek, S., Vuister, G. W., Zhu, G., Pfeifer, J., and Bax, A. (1995) NMRPipe: a multidimensional spectral processing system based on UNIX pipes. *J. Biomol. NMR* **6,** 277–293
37. Johnson, B. A., and Blevins, R. A. (1994) NMRView: a computer program for the visualization and analysis of NMR data. *J. Biomol. NMR* **4,** 603–614
38. Hudson, R. P., Chong, P. A., Protasevich, I. I., Vernon, R., Noy, E., Bihler, H., An, J. L., Kalid, O., Sela-Culang, I., Mense, M., Senderowitz, H., Brouillette, C. G., and Forman-Kay, J. D. (2012) Conformational changes relevant to channel activity and folding within the first nucleotide binding domain of CFTR. *J. Biol. Chem.* **287,** 28480–28494
39. Kanelis, V., Forman-Kay, J. D., and Kay, L. E. (2001) Multidimensional NMR methods for protein structure determination. *IUBMB Life* **52,** 291–302
40. Sattler, M., Schleucher, J., and Griesinger, C. (1999) Heteronuclear multidimensional NMR experiments for the structure determination of proteins in solution employing pulsed field gradients. *Prog. Nuclear Magn. Reson. Spectrosc.* **34,** 93–158
41. Smith, S. P., Barber, K. R., and Shaw, G. S. (1997) Identification and structural influence of a differentially modified N-terminal methionine in human S100b. *Protein Sci.* **6,** 1110–1113
42. Atreya, H. S. (2012) in *Isotope Labelling in Biomolecular NMR* (Atreya, H., ed) Springer-Verlag, Inc., New York
43. Krishnarjuna B., Jaipuria G., Thakur A., D'Silva P., and Atreya H. S. (2011) Amino acid selective unlabeling for sequence specific resonance assignments in proteins. *J. Biomol. NMR* **49,** 39–51
44. López-Alonso, J. P., de Araujo, E. D., and Kanelis, V. (2012) NMR and fluorescence studies of drug binding to the first nucleotide binding domain of SUR2A. *Biochemistry* **51,** 9211–9222
45. Pain, R. H. (2005) Determining the fluorescence spectrum of a protein. *Curr. Protoc. Protein Sci.* Chapter 7, Unit 7.7
46. Guarnieri, M. T., Blagg, B. S., and Zhao, R. (2011) A high-throughput TNP-ATP displacement assay for screening inhibitors of ATP-binding in bacterial histidine kinases. *Assay Drug Dev. Technol.* **9,** 174–183
47. Viguera, A. R., Arrondo, J. L., Musacchio, A., Saraste, M., and Serrano, L. (1994) Characterization of the interaction of natural proline-rich peptides with five different SH3 domains. *Biochemistry* **33,** 10925–10933
48. Csanády, L., Chan, K. W., Seto-Young, D., Kopsco, D. C., Nairn, A. C., and Gadsby, D. C. (2000) Severed channels probe regulation of gating of cystic fibrosis transmembrane conductance regulator by its cytoplasmic domains. *J. Gen. Physiol.* **116,** 477–500
49. Karger, A. B., Park, S., Reyes, S., Bienengraeber, M., Dyer, R. B., Terzic, A., and Alekseev, A. E. (2008) Role for SUR2A ED domain in allosteric coupling within the K(ATP) channel complex. *J. Gen. Physiol.* **131,** 185–196
50. Cuthbertson, J. M., Doyle, D. A., and Sansom, M. S. (2005) Transmembrane helix prediction: a comparative evaluation and analysis. *Protein Eng. Des. Sel.* **18,** 295–308
51. Aller, S. G., Yu, J., Ward, A., Weng, Y., Chittaboina, S., Zhuo, R., Harrell, P. M., Trinh, Y. T., Zhang, Q., Urbatsch, I. L., and Chang, G. (2009) Structure of P-glycoprotein reveals a molecular basis for poly-specific drug binding. *Science* **323,** 1718–1722
52. Dawson, R. J., and Locher, K. P. (2006) Structure of a bacterial multidrug ABC transporter. *Nature* **443,** 180–185
53. Hohl, M., Briand, C., Grütter, M. G., and Seeger, M. A. (2012) Crystal structure of a heterodimeric ABC transporter in its inward-facing conformation. *Nat. Struct. Mol. Biol.* **19,** 395–402
54. Hollenstein, K., Dawson, R. J., and Locher, K. P. (2007) Structure and mechanism of ABC transporter proteins. *Curr. Opin. Struct. Biol.* **17,** 412–418
55. Jin, M. S., Oldham, M. L., Zhang, Q., and Chen, J. (2012) Crystal structure of the multidrug transporter P-glycoprotein from *Caenorhabditis elegans*. *Nature* **490,** 566–569
56. Shintre, C. A., Pike, A. C., Li, Q., Kim, J. I., Barr, A. J., Goubin, S., Shrestha, L., Yang, J., Berridge, G., Ross, J., Stansfeld, P. J., Sansom, M. S., Edwards, A. M., Bountra, C., Marsden, B. D., *et al.* (2013) Structures of ABCB10, a human ATP-binding cassette transporter in apo- and nucleotide-bound states. *Proc. Natl. Acad. Sci. U.S.A.* **110,** 9710–9715
57. Ward, A., Reyes, C. L., Yu, J., Roth, C. B., and Chang, G. (2007) Flexibility in the ABC transporter MsbA: alternating access with a twist. *Proc. Natl. Acad. Sci. U.S.A.* **104,** 19005–19010
58. Li, X., Romero, P., Rani, M., Dunker, A. K., and Obradovic, Z. (1999) Predicting Protein Disorder for N-, C-, and Internal Regions. *Genome Inform. Ser. Workshop Genome Inform.* **10,** 30–40
59. Romero, Obradovic, and Dunker, K. (1997) Sequence data analysis for long disordered regions prediction in the calcineurin family. *Genome Inform. Ser. Workshop Genome Inform.* **8,** 110–124
60. Romero, P., Obradovic, Z., Li, X., Garner, E. C., Brown, C. J., and Dunker, A. K. (2001) Sequence complexity of disordered protein. *Proteins* **42,** 38–48
61. Kanelis, V., Chong, P. A., and Forman-Kay, J. D. (2011) NMR spectroscopy to study the dynamics and interactions of CFTR. *Methods Mol. Biol.* **741,** 377–403
62. Pearson, R. B., and Kemp, B. E. (1991) Protein kinase phosphorylation site sequences and consensus specificity motifs: tabulations. *Methods Enzymol.* **200,** 62–81
63. Rust, H. L., and Thompson, P. R. (2011) Kinase consensus sequences: a breeding ground for crosstalk. *ACS Chem. Biol.* **6,** 881–892
64. Grifman, M., Arbel, A., Ginzberg, D., Glick, D., Elgavish, S., Shaanan, B., and Soreq, H. (1997) *In vitro* phosphorylation of acetylcholinesterase at nonconsensus protein kinase A sites enhances the rate of acetylcholine hydrolysis. *Brain Res. Mol. Brain Res.* **51,** 179–187
65. Hirling, H., and Scheller, R. H. (1996) Phosphorylation of synaptic vesicle proteins: modulation of the α SNAP interaction with the core complex. *Proc. Natl. Acad. Sci. U.S.A.* **93,** 11945–11949
66. Ubersax, J. A., Woodbury, E. L., Quang, P. N., Paraz, M., Blethrow, J. D., Shah, K., Shokat, K. M., and Morgan, D. O. (2003) Targets of the cyclin-dependent kinase Cdk1. *Nature* **425,** 859–864
67. Walsh, D. A., and Van Patten, S. M. (1994) Multiple pathway signal transduction by the cAMP-dependent protein kinase. *FASEB J.* **8,** 1227–1236
68. Chen, J., Lu, G., Lin, J., Davidson, A. L., and Quiocho, F. A. (2003) A tweezers-like motion of the ATP-binding cassette dimer in an ABC transport cycle. *Mol. Cell* **12,** 651–661
69. Karpowich, N., Martsinkevich, O., Millen, L., Yuan, Y. R., Dai, P. L., MacVey, K., Thomas, P. J., and Hunt, J. F. (2001) Crystal structures of the MJ1267 ATP binding cassette reveal an induced-fit effect at the ATPase active site of an ABC transporter. *Structure* **9,** 571–586
70. Verdon, G., Albers, S. V., van Oosterwijk, N., Dijkstra, B. W., Driessen, A. J., and Thunnissen, A. M. (2003) Formation of the productive ATP-Mg^{2+}-bound dimer of GlcV, an ABC-ATPase from *Sulfolobus solfataricus*. *J. Mol. Biol.* **334,** 255–267
71. Yuan, Y. R., Blecker, S., Martsinkevich, O., Millen, L., Thomas, P. J., and Hunt, J. F. (2001) The crystal structure of the MJ0796 ATP-binding cassette. Implications for the structural consequences of ATP hydrolysis in the active site of an ABC transporter. *J. Biol. Chem.* **276,** 32313–32321
72. Mittag, T., Kay, L. E., and Forman-Kay, J. D. (2010) Protein dynamics and conformational disorder in molecular recognition. *J. Mol. Recognit.* **23,** 105–116
73. Pufall, M. A., Lee, G. M., Nelson, M. L., Kang, H. S., Velyvis, A., Kay, L. E., McIntosh, L. P., and Graves, B. J. (2005) Variable control of Ets-1 DNA

binding by multiple phosphates in an unstructured region. *Science* **309,** 142–145
74. Yamada, M., Ishii, M., Hibino, H., and Kurachi, Y. (2004) Mutation in nucleotide-binding domains of sulfonylurea receptor 2 evokes Na-ATP-dependent activation of ATP-sensitive K^+ channels: implication for dimerization of nucleotide-binding domains to induce channel opening. *Mol. Pharmacol.* **66,** 807–816
75. Bienengraeber, M., Alekseev, A. E., Abraham, M. R., Carrasco, A. J., Moreau, C., Vivaudou, M., Dzeja, P. P., and Terzic, A. (2000) ATPase activity of the sulfonylurea receptor: a catalytic function for the K_{ATP} channel complex. *FASEB J.* **14,** 1943–1952
76. Masia, R., Enkvetchakul, D., and Nichols, C. G. (2005) Differential nucleotide regulation of K_{ATP} channels by SUR1 and SUR2A. *J. Mol. Cell. Cardiol.* **39,** 491–501
77. MacArthur, M. W., and Thornton, J. M. (1991) Influence of proline residues on protein conformation. *J. Mol. Biol.* **218,** 397–412
78. Deber, C. M., Brodsky, B., and Rath, A. (2010) *Proline Residues in Proteins*, John Wiley & Sons Ltd., Chichester, UK
79. Chutkow, W. A., Simon, M. C., Le Beau, M. M., and Burant, C. F. (1996) Cloning, tissue expression, and chromosomal localization of SUR2, the putative drug-binding subunit of cardiac, skeletal muscle, and vascular K_{ATP} channels. *Diabetes* **45,** 1439–1445
80. Ortiz, D., Gossack, L., Quast, U., and Bryan, J. (2013) Reinterpreting the action of ATP analogs on K(ATP) channels. *J. Biol. Chem.* **288,** 18894–18902
81. Stolarczyk, E. I., Reiling, C. J., and Paumi, C. M. (2011) Regulation of ABC transporter function via phosphorylation by protein kinases. *Curr. Pharm. Biotechnol.* **12,** 621–635
82. Roosbeek, S., Peelman, F., Verhee, A., Labeur, C., Caster, H., Lensink, M. F., Cirulli, C., Grooten, J., Cochet, C., Vandekerckhove, J., Amoresano, A., Chimini, G., Tavernier, J., and Rosseneu, M. (2004) Phosphorylation by protein kinase CK2 modulates the activity of the ATP binding cassette A1 transporter. *J. Biol. Chem.* **279,** 37779–37788
83. See, R. H., Caday-Malcolm, R. A., Singaraja, R. R., Zhou, S., Silverston, A., Huber, M. T., Moran, J., James, E. R., Janoo, R., Savill, J. M., Rigot, V., Zhang, L. H., Wang, M., Chimini, G., Wellington, C. L., *et al.* (2002) Protein kinase A site-specific phosphorylation regulates ATP-binding cassette A1 (ABCA1)-mediated phospholipid efflux. *J. Biol. Chem.* **277,** 41835–41842
84. Sharom, F. J. (2011) The P-glycoprotein multidrug transporter. *Essays Biochem.* **50,** 161–178
85. Cheng, S. H., Rich, D. P., Marshall, J., Gregory, R. J., Welsh, M. J., and Smith, A. E. (1991) Phosphorylation of the R domain by cAMP-dependent protein kinase regulates the CFTR chloride channel. *Cell* **66,** 1027–1036
86. Picciotto, M. R., Cohn, J. A., Bertuzzi, G., Greengard, P., and Nairn, A. C. (1992) Phosphorylation of the cystic fibrosis transmembrane conductance regulator. *J. Biol. Chem.* **267,** 12742–12752
87. Tabcharani, J. A., Chang, X. B., Riordan, J. R., and Hanrahan, J. W. (1991) Phosphorylation-regulated Cl^- channel in CHO cells stably expressing the cystic fibrosis gene. *Nature* **352,** 628–631
88. Lewis, H. A., Buchanan, S. G., Burley, S. K., Conners, K., Dickey, M., Dorwart, M., Fowler, R., Gao, X., Guggino, W. B., Hendrickson, W. A., Hunt, J. F., Kearins, M. C., Lorimer, D., Maloney, P. C., Post, K. W., *et al.* (2004) Structure of nucleotide-binding domain 1 of the cystic fibrosis transmembrane conductance regulator. *EMBO J.* **23,** 282–293
89. Hegedus, T., Serohijos, A. W., Dokholyan, N. V., He, L., and Riordan, J. R. (2008) Computational studies reveal phosphorylation-dependent changes in the unstructured R domain of CFTR. *J. Mol. Biol.* **378,** 1052–1063
90. Zhang, L., Aleksandrov, L. A., Zhao, Z., Birtley, J. R., Riordan, J. R., and Ford, R. C. (2009) Architecture of the cystic fibrosis transmembrane conductance regulator protein and structural changes associated with phosphorylation and nucleotide binding. *J. Struct. Biol.* **167,** 242–251
91. Aleksandrov, A. A., Kota, P., Aleksandrov, L. A., He, L., Jensen, T., Cui, L., Gentzsch, M., Dokholyan, N. V., and Riordan, J. R. (2010) Regulatory insertion removal restores maturation, stability and function of ΔF508 CFTR. *J. Mol. Biol.* **401,** 194–210
92. Drumm, M. L., Wilkinson, D. J., Smit, L. S., Worrell, R. T., Strong, T. V., Frizzell, R. A., Dawson, D. C., and Collins, F. S. (1991) Chloride conductance expressed by ΔF508 and other mutant CFTRs in *Xenopus* oocytes. *Science* **254,** 1797–1799
93. Wang, F., Zeltwanger, S., Hu, S., and Hwang, T. C. (2000). Deletion of phenylalanine 508 causes attenuated phosphorylation-dependent activation of CFTR chloride channels. *J. Physiol.* **524,** 637–648
94. Schultz, B. D., Frizzell, R. A., and Bridges, R. J. (1999) Rescue of dysfunctional deltaF508-CFTR chloride channel activity by IBMX. *J. Membr. Biol.* **170,** 51–66
95. Ramaen, O., Leulliot, N., Sizun, C., Ulryck, N., Pamlard, O., Lallemand, J. Y., Tilbeurgh Hv, and Jacquet, E. (2006) Structure of the human multidrug resistance protein 1 nucleotide binding domain 1 bound to Mg^{2+}/ATP reveals a nonproductive catalytic site. *J. Mol. Biol.* **359,** 940–949
96. Koradi, R., Billeter, M., and Wüthrich, K. (1996) MOLMOL: a program for display and analysis of macromolecular structures. *J. Mol. Graph.* **14,** 51–5532